Journal of Controlled Release 382 (2025) 113679

Contents lists available at ScienceDirect

Journal of Controlled Release

journal homepage: www.elsevier.com/locate/jconrel

DNA scaffold-framed natural killer cell with programmed drug release for chemo-adoptive cell therapy

Shiyi Bi [a], Jieyu Shen [a], Yu Zhu [a], Lei Fan [c], Huangxian Ju [a], Ying Liu [a,b,*]

[a] State Key Laboratory of Analytical Chemistry for Life Science, School of Chemistry and Chemical Engineering, Nanjing University, Nanjing 210023, China
[b] Chemistry and Biomedicine Innovation Center, Nanjing University, Nanjing 210023, China
[c] Department of Hematology, The First Affiliated Hospital of Nanjing Medical University, Jiangsu Province Hospital, Collaborative Innovation Center for Cancer Personalized Medicine, Nanjing 210023, China

ARTICLE INFO

Keywords:
DNA scaffold
NK cells
Chemotherapy
Adoptive cell therapy
Programmable drugs release

ABSTRACT

Choosing appropriate delivery system for chemotherapeutic drugs as well as arranging the time spots for adoptive cells administrations is the key to achieve efficient combined chemo-adoptive cell therapy. Tumor-homing character makes adoptive immune cells appropriate targeting delivery carriers, but they are rarely used for chemtoxic payloads considering payloads internalization during administration which impairs adoptive cells. Herein, we frame adoptive NK cells using DNA scaffold with chemotherapeutic payloads fastened exterior, and achieves time-programmed drugs release and NK cell decapsulation to minimize side effects and enhance therapeutic effect. IL-21 nanoparticles are prepared by conjugating cytokine IL-21 with a GSH cleavable linker and act as anchor points for DNA scaffold assembly. Chemotherapeutic payloads are prepared by loading DOX/verapamil drugs to PLGA nanoparticles ($PLGA_{drugs}$ NPs), and connected to the exterior of DNA scaffold with a ROS cleavable linker. Porous DNA scaffold protects NK cells functions from impairing by chemotherapeutic payloads, while guarantees efficient communication of NK cells with exterior environment to keep tumor homing capability. Reactive oxygen species (ROS) in tumor microenvironment releases $PLGA_{drugs}$ NPs to perform chemotherapy, which subsequently generates a reductive environment to detach DNA scaffold for NK cell and IL-21 release to achieve combined chemo-adoptive cell therapy with enhanced therapeutic efficiency.

1. Introduction

Adoptive cell based immunotherapy (ACT), which involves the administration of immune cells as living agents to fight disease, holds remarkable advantages in many cancer treatments [1–3] with promising clinical translation potentials [4–7]. Despite these achievements, a major limitation of adoptive cells based immunotherapy is the rapid function decline of transplanted immune cells [8] due to the immunosuppressive tumor microenvironment and corresponding inadequate immune cells infiltration and activation [9–11].

The combination of chemotherapy and immunotherapy is now becoming a part of the standard care [12–14] with over hundreds of clinical trials verified treatment efficiency enhancement [15]. Chemotherapy induces immunogenic cell death (ICD) and remodels immunosuppressive tumor microenvironment, which provides substantial contribution to immunotherapy [16,17]. However, the combination of chemotherapy with adoptive cell therapy still faces challenges. The cytotoxic effects of chemotherapeutic drugs may also have a deleterious effect on adoptive cell viability and function [18,19], its systemic delivery may also have side effects on normal tissues [20–22]. Therefore, choosing the appropriate delivery system for chemotherapeutic drugs as well as arranging the time spots for adoptive cells administrations is the key to achieve combined chemo-adoptive cell therapy.

Tumor-homing characteristic of adoptive immune cells makes them good targeting delivery carriers [23–26]. "Backpacking" strategies [23] that conjugated immunostimulatory cytokines as payloads have been reported to enhance the killing or antigen presentation abilities of adoptive immune cells [27–30]. However, it is challenging to extend the "backpacked" payloads to cytotoxic chemotherapeutic drugs. Considering the dynamic of plasma membrane, retaining payloads at adoptive immune cell membrane during systematic circulation process is difficult [31], and the internalization of chemotherapeutic drugs into the

* Corresponding author at: State Key Laboratory of Analytical Chemistry for Life Science, School of Chemistry and Chemical Engineering, Nanjing University, Nanjing 210023, China.
E-mail address: yingliu@nju.edu.cn (Y. Liu).

https://doi.org/10.1016/j.jconrel.2025.113679
Received 15 December 2024; Received in revised form 30 March 2025; Accepted 31 March 2025
Available online 1 April 2025

cytoplasm of immune cell would highly impair their viabilities and functions [32,33]. Currently reported chemotherapy drugs loaded adoptive cells [34] and artificial cells that wrapped with natural cell membrane [35,36] usually demonstrated tumor-homing capability for leading chemotherapy drugs to destinations, but rarely showed immunoactivity.

Taking advantages of self-assembled DNA nanostructures, herein, we develop a "non-direct contact" backpacking strategy to conjugate chemotherapeutic drugs and immunostimulatory cytokines to adoptive cells, as well as programming their "on-demand" sequential release of

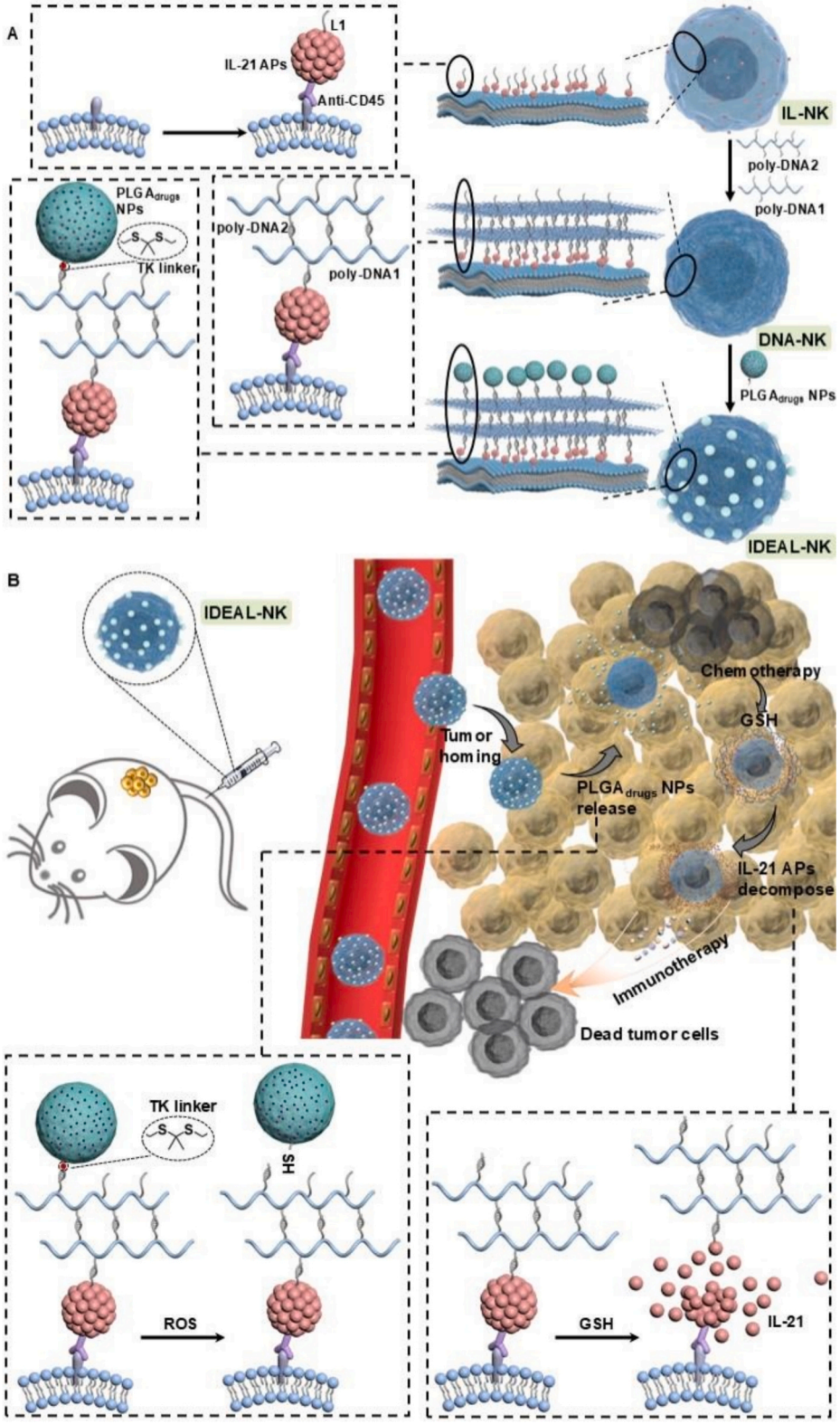

Scheme 1. Schematic illustration of DNA scaffold framed adoptive natural killer cells with therapeutic effect enhancement. (A) Preparation of IDEAL-NK cells. (B) Sequential release of drugs and IL-21 for chemotherapy boosted adoptive cell therapy.

chemotherapeutic drugs and decapsulation of adoptive cells at tumor position. Considering natural killer (NK) cells' superior safety (such as reducing risks of cytokine release syndrome and neurotoxicity), MHC-unrestricted solid tumor cytotoxicity, and multimodal antitumor mechanisms, they were selected as the adoptive cell model [37–39]. Adoptive NK cells are framed with a DNA-hydrogel scaffold, and back-packed with payloads chemotherapeutic drug doxorubicin (DOX)/verapamil and immunostimulatory cytokine interleukin 21 (IL-21) at the exterior and interior of the scaffold, respectively. The chemotherapeutic payload and immuno-booster payload are programmed for sequential release to achieve combined treatment of chemotherapy and adoptive cell based immunotherapy, which remodels the tumor microenvironment and enhances the efficacy of adoptive NK cell therapy. IL-21 anchoring nanoparticles (IL-21 APs), which serve not only as structural anchors for stable DNA scaffold assembly but also as immuno-booster payloads [40] that activate NK cells upon disassembly, are prepared by crosslinking cytokine IL-21 with NHS-SS-NHS and modified with DNA strand L1 and CD45 antibody (Anti-CD45). IL-21 APs attach to NK cells upon recognizing membrane CD45 receptor and act as anchor points to construct DNA scaffold around NK cell (Scheme 1A, IL-NK). Poly-DNA1 and poly-DNA2 with complementary sequence, are synthesized by polymerizing acrydite-modified nucleic acids strands respectively, and serve as components for DNA scaffold. Poly-DNA1 is linked to IL-21 APs first via hybridization with DNA strand L1, and sequentially hybridized with poly-DNA2 to construct Acryl-DNA scaffold framed NK cells (Scheme 1A, DNA-NK). The chemotherapeutic payload, $PLGA_{drugs}$ nanoparticles ($PLGA_{drugs}$ NPs) that encapsulated with DOX and verapamil, were synthesized via nanoprecipitation method and modified with DNA strand N1 via ROS-responsive thioketal (TK) linkers, which act as DOX reservoir and are connected to DNA-NK via hybridization with poly-DNA2 to obtain IL-21 and Drug Equipped AcryL-DNA scaffold framed NK cells (Scheme 1A, IDEAL-NK).

The as-obtained DNA scaffold has pore size around ~100 nm, which doesn't affect chemokine signal transmission, and the corresponding tumor homing capability of IDEAL-NK cells guides it through systematic circulation to locate to tumor sites (Scheme 1B, tumor homing). DNA scaffold framing effectively isolates NK cell from $PLGA_{drugs}$ NPs, which prevents drug-induced toxicity damage to NK cells in systematic circulation process. Overexpressed ROS at tumor microenvironment cleaves TK linker to release $PLGA_{drugs}$ NPs from IDEAL-NK cell (Scheme 1B, $PLGA_{drugs}$ NPs release). DNA scaffold on IDEAL-NK cells remains intact during $PLGA_{drugs}$ NPs release process, which blocks the access of $PLGA_{drugs}$ NPs to NK cells. The released $PLGA_{drugs}$ NPs are endocytosed by tumor cells, which subsequently degrades in phagosome environment with low pH and hydrolytic enzymes [41] to release drugs DOX for chemotherapy and verapamil for glutathione (GSH) efflux to boost chemotherapy (Scheme 1B, chemotherapy). GSH efflux enhances local reducing environment, cleaves disulfide bonds in IL-21 APs (Scheme 1B, IL-21 APs decompose), which not only generates IL-21 in situ to remodel the immunosuppressed microenvironment, but also liberates NK cells.

from DNA frame for immunotherapy. The released IL-21 promotes NK cell proliferation and activation, thus enhances immunotherapy efficiency (Scheme 1B, immunotherapy). The as-obtained IDEAL-NK cells prevent direct contact of chemotherapeutic drugs with NK cells in systematic circulation, and program sequential release of drugs and IL-21 to achieve combined chemo-immunotherapy. Chemotherapy, as the preceding process, effectively depletes immunosuppressive cells, promotes a pro-inflammatory tumor microenvironment, and promotes infiltration of adoptive NK cells [42–46], which results in its outstanding tumor cell killing capacity, indicating clinic application potential.

2. Materials and methods

2.1. Materials

Acrylamide, ammonium persulphate (APS), *N*,*N*,*N*′,*N*′-Tetramethylethylenediamine (TEMED), and poly(2-hydroxyethyl methacrylate) (pHEMA) were purchased from Sigma-Aldrich (USA). NHS-SS-NHS was purchased from Xi'an ruixi Biological Technology Co., Ltd. (Xi'an, China). IL-21 was purchased from Sino Biological Inc. (Beijing, China). Polyvinyl alcohol (PVA) was purchased from Sinopharm Chemical Reagent Co., Ltd. (Shanghai,China). Dichloromethane (DCM) was purchased from J&K Chemical Technology (Beijing, China). Doxorubicin (DOX) and verapamil hydrochloride were purchased from Aladdin Biochemistry Technology Co., Ltd. (Shanghai, China). Trypsin, fetal bovine serum, RPMI 1640 medium, MTT assay Kit, phosphate buffer solution (PBS), and human lung adenocarcinoma cell line A549 were purchased from Keygen Biotech (Nanjing, China). CD45 antibody was purchased from Thermo Fisher Scientific (USA). Annexin V-fluorescein isothiocyanate (FITC)/DAPI apoptosis detection kit, interleukin-2 (IL-2), granzyme B (GzmB), and tumor necrosis factor α (TNF-α) ELISA kits were purchased from Elabscience Biotechnology Co., Ltd. (Wuhan, China). α-MEM medium, NK-92MI cells were purchased from Wuhan Pricella Biotechnology Co., Ltd. (Wuhan, China). All DNAs were synthesized and purified by Sangon Biotech Co., Ltd. (Shanghai, China). The sequences for all DNA strands were listed in Table S1.

2.2. Apparatus

JEM-2100 transmission electron microscope (JEOL, Japan) and JSM-7800F thermal field emission scanning electron microscope (JEOL, Japan) were used to obtain transmission electron microscope (TEM) images and scanning electron microscope (SEM) images, respectively. SCIENTZ-IID ultrasonic crusher (Ningbo, China) was used for ultrasonic emulsification. Nano-Z Zeta (Malvern Panalytical, UK) was used for zeta potential determination. ZetaPlus 90 Plus/BI-MAS (Brookhaven, USA) was used for dynamic light scattering (DLS) analysis. Cell images were obtained on a Leica SP8 STED 3× confocal microscope (Germany). Flow cytometric analysis was performed on the CytoFlex S flow cytometer (Beckman-Coulter, USA). In vivo mice imaging was performed on IVIS Lumina XR III in vivo imaging system (PerkinElmer, USA).

2.3. Preparation of IL-21 APs

IL-21 nanoparticles (IL-21 NPs) were prepared by self-assembling IL-21 protein. NHS-SS-NHS (0.1 mg/mL, 25 μL) was mixed with IL-21 (6.6 μM, 50 μL), complemented with PBS to 1 mL, and rotated at room temperature for 30 min. Subsequently, anti-CD45 (10 μL, 0.25 mg/mL) and NH_2-modified DNA strand L1 (10 μL, 50 μM) were added to the above mixture and continuously rotated for another 30 min to obtain IL-21 anchoring nanoparticles (IL-21 APs). The as-obtained IL-21 APs were washed with PBS in an ultra-filtration centrifuge tube (molecular weight cut-off =100 kDa, Millipore, USA) for three times. The filtered liquid was collected and supplemented with PBS to 200 μL.

2.4. In vitro characterization of IL-21 APs decompose

The above prepared IL-21 APs were decomposed in response to GSH to release IL-21. ELISA was used to determine the percentage of IL-21 release from IL-21 APs. Briefly, IL-21 APs were dispersed in PBS (1 mL) buffer and put into a dialysis bag (MW35000). Then dialysis bags were placed in 5 mL PBS (5 mL) with 1 mM GSH. 100 μL of PBS outside the dialysis bag was collected at selected time intervals for ELISA analysis. Control group was prepared with the same procedure in the absence of GSH.

2.5. Preparation of $PLGA_{drugs}$ NPs

DOX/verapamil-loaded PEG-PLGA NPs ($PLGA_{drugs}$ NPs) were prepared by nanoprecipitation. PLGA-PEG-NH_2 and mPEG-PLGA (3:7 weight ratio) were dissolved in DCM with a final concentration of 20 mg/mL. The mixture was emulsified by sonication with a probe

ultrasonicator at 25 % power for 5 min. 0.2 mL of DOX/verapamil (1 mg) was then dissolved in DCM with 2 mL of 2 % (*w/v*) PVA, the mixture solution was emulsified again by sonication at 30 % power for another 5 min. The as-obtained drugs dispersed DCM solution was added dropwisely to 10 mL 0.6 % (w/v) PVA and stirred for 3 min. The organic solvent was removed from the mixture by gentle stirring for 6 h, and drugs loaded PLGA nanoparticles were collected by centrifugation at 15,000 *g* for 5 min followed with freeze-drying.

DNA strand N1 was then connected to drugs loaded PLGA nanoparticles via a ROS responsive linker NHS-TK-NHS. NHS-TK-NHS was synthesized by mixing 2,2′-[propane-2,2-diylbis(thio)] diacetic acid (2.5 mg), NHS (2.5 mg) and EDC (3.5 mg) in DMSO and stirred at room temperature for 6 h. 50 μL of the as-obtained NHS-TK-NHS solution was pipetted into 100 μL NH_2 functionalized DNA strand N1 solution (50 μM) and stirred for 30 min at room temperature. The as-obtained mixture solution was subsequently ultrafiltrated (MWCO of 3 kDa) to remove unreacted NHS-TK-NHS, subsequently mixed with 200 μL of above obtained drugs loaded PLGA nanoparticles, and stirred at room temperature for another 2 h to obtain $PLGA_{drugs}$-N1 NPs.

2.6. Preparation of poly-DNAs

Poly-DNAs were prepared by *co*-polymerization of acrydite-modified DNA strands. 150 μL buffer solution (Tris-HCl, 10 mM, pH 8.0) containing 3 % acrylamide and 50 μM acrydite-modified DNA strands P1a, P1b, P1c was bubbled with nitrogen through the solutions. 2.8 μL of 10 % APS solution and 0.4 μL TEMED was then added in, the as-obtained mixture solutions were allowed to polymerize at room temperature for 5 min and at 4 °C for 12 h. The resulting copolymers were ultrafiltrated (MWCO = 10 kDa) to remove unreacted monomer units, salts, and initiator, and dissolved in 200 μL water for subsequent use. The concentration of poly-DNAs was defined according to the concentration of component DNA strands. Poly-DNA1 was prepared with acrylamide and P1a, P1b, P1c as components, and poly-DNA2 was prepared with acrylamide and P2a, P2b, P2c as components. P1a has complementary sequences with DNA strand L1, P1b and P1c have complementary sequences with P2b and P2c, respectively.

2.7. Cell culture

NK-92MI cells were cultured in MEM-α medium supplemented with 0.2 mM inositol, 0.1 mM β-mercaptoethanol, 0.02 mM folic acid, 12.5 % horse serum, 12.5 % fetal bovine serum, and 100 mg/mL streptomycin and penicillin. A549 cells were cultured in an RPMI-1640 medium complemented with 10 % FBS, 100 mg/mL streptomycin and penicillin. All cells were grown at 37 °C in a humidified atmosphere containing 5 % CO_2. Cell numbers were counted by a Countess II FL Automated Cell Counter (Thermo Fisher Scientific).

2.8. Preparation of IDEAL-NK cells

IL-21 and Drugs Equipped AcryL-DNA scaffold framed NK cells (IDEAL-NK cells) were prepared by framing NK cells with DNA scaffolds and loading $PLGA_{drugs}$ NPs to DNA scaffolds. The above obtained IL-21 APs were incubated with NK-92MI cells in 1640 medium for 30 min to allow specific recognition and binding of anti CD45, which modified on IL-21 APs surface, to CD45 that highly expressed on NK-92 cell membrane, followed by rinsing with 1640 medium for three times to remove unbound IL-21 APs to obtain IL-NK cells.

The DNA frame was then assembled on the above-obtained IL-NK cells. IL-NK cells were then sequentially incubated with poly-DNA1 and poly-DNA2 for 30 min respectively, washed for three times to remove unreacted poly-DNA strands to obtain AcryL-DNA scaffold encapsulated NK (DNA-NK) cells. The as-obtained DNA-NK cells were subsequently incubated with $PLGA_{drugs}$-N1 at 37 °C for 30 min, and washed with 1640 medium to obtain IDEAL-NK cells.

2.9. The loading efficiency of $PLGA_{drugs}$ NPs to IDEAL-NK cells

To measure the content of $PLGA_{drugs}$ NPs loaded on IDEAL-NK cells, fluorescence calibration curves of $PLGA_{drugs}$ NPs were achieved first by measuring fluorescence intensities of various concentrations of $PLGA_{drugs}$ NPs at 593 nm. The concentration of $PLGA_{drugs}$ NPs was determined by a standard calibration curve. The freshly prepared DNA-NK cells were incubated with $PLGA_{drugs}$-N1 NPs for 30 min, centrifuged at 800 rpm for 5 min. The extra $PLGA_{drugs}$ NPs that didn't load to IDEAL-NK cells were determined by measuring supernatant fluorescence at 593 nm. The as-obtained unloaded $PLGA_{drugs}$ NPs were subtracted from that of $PLGA_{drugs}$ NPs incubated with IDEAL-NK cells, and divided with incubated cell number to calculate the loaded amount of $PLGA_{drugs}$ NPs to IDEAL-NK cells.

2.10. In vitro characterization of sequential DNA scaffold decapsulation and liberation of NK cells

To verify the ROS responsive release of $PLGA_{drugs}$ NPs from IDEAL-NK cells and NK-$PLGA_{drugs}$ cells, 1×10^5 IDEAL-NK cells or NK-$PLGA_{drugs}$ cells were cultured in 1640 medium with H_2O_2 (200 μM) for 2 h and washed three times to obtain DNA-NK cells before CLSM imaging.

To verify the location of $PLGA_{drugs}$ NPs after its release from IDEAL-NK cells, A549 cells were seeded at a cell density of 1×10^5 per well in confocal dishes for 16 h, subsequently co-cultured with IDEAL-NK cells in 1640 medium with H_2O_2 (2 mM) for 0.5 h. The liberated $PLGA_{drugs}$ NPs were visualized via DOX fluorescence under CLSM with excitation wavelength of 480 nm and emission wavelength of 580 nm. Control experiment was performed with the same procedure in the absence of H_2O_2.

To continuously monitor GSH-responsive decapsulation of DNA scaffold and release of NK cells, the above obtained DNA-NK cells were resuspended in 1640 medium containing GSH (10 mM), incubated for 0.5 h and washed three times. The liberated NK cells were visualized via FAM and Cy5 fluorescence under CLSM.

2.11. In vitro proliferation assay of DNA-NK cells

NK cells were stained with CFSE (1 μg/mL) at 37 °C for 20 min, assembled with IL-21 APs and poly-DNAs according to the same procedure described above to obtain DNA-NK_{CFSE} cells. The as-obtained DNA-NK_{CFSE} cells were resuspended in 1640 medium for 2 days in the presence and absence of GSH (5 mM) respectively, and the cell proliferation was characterized by measuring CFSE fluorescence intensity changes with flow cytometry. Control experiment was performed with the same procedure using CFSE stained naked NK cells without DNA scaffold.

2.12. Migration characterization of IDEAL-NK cells

Migration of IDEAL-NK cells was evaluated using Transwell chamber. 1×10^5 IDEAL-NK cells that prepared with different concentrations of poly-DNAs (0 nM, 500 nM, and 5 μM) were added to the upper chamber. A549 cells were seeded in the lower chamber which provided chemotaxis stimulus for IDEAL-NK cells migration. After 24 h incubation, IDEAL-NK cells that migrated to the lower chamber were photographed by confocal microscope.

2.13. In vitro evaluation of $PLGA_{drugs}$ NPs cytotoxicity to IDEAL-NK cells

The cytotoxicity of $PLGA_{drugs}$ NPs to NK cells was evaluated by measuring NK cell viability. 1×10^5 DNA-NK cells that prepared with different concentrations of poly-DNAs (0 nM, 500 nM, and 5 μM) were incubated with $PLGA_{drugs}$-N1 NPs for 24 h and cell viability was evaluated according to the MTT assay manufacturer's instructions.

To further visualize the location of $PLGA_{drugs}$ NPs on IDEAL-NK cells,

1×10^5 DNA-NK cells that prepared with different concentrations of poly-DNAs (0 nM, 500 nM, and 5 μM) were co-cultured with $PLGA_{drugs}$-N1 NPs for 8 h and then washed three times for CLSM imaging. The fluorescence of DOX with excitation wavelength of 480 nm and emission wavelength of 580 nm was taken to indicate the location of $PLGA_{drugs}$ NPs.

2.14. In vitro characterization of killing capability for IDEAL-NK cells

MTT assay and Annexin V-FITC/DAPI apoptosis analysis were performed to evaluate the killing capability of IDEAL-NK cells to tumor cells. IL-NK cells that only have IL-21 APs anchored to NK cells, and NK-$PLGA_{drugs}$ cells were set as control groups. NK-$PLGA_{drugs}$ cells were prepared by directly hybridizing $PLGA_{drugs}$-N1 NPs with IL'-NK cells that anchored with IL-21 APs'. IL-21 APs' were prepared with DNA strand L1' instead of L1, where L1' hybridized with N1 for $PLGA_{drugs}$ NPs attachment without DNA scaffold. NK-$PLGA_{drugs}$ cells, and IDEAL-NK cells were incubated with A549 cells respectively for 48 h. MTT assay was performed by measuring absorption at 490 nm.

The apoptosis of A549 cells for different treatment groups was evaluated by flow cytometry. A549 cells that treated with IL-NK cells, NK-$PLGA_{drugs}$ cells and IDEAL-NK cells respectively were washed three times with PBS, digested with EDTA-free trypsin, and stained with Annexin V-FITC/DAPI assay kit for cell apoptosis analysis.

2.15. In vivo imaging of IDEAL-NK cells

A549-bearing BABL/C nude mice were used for the in vivo study. All in vivo procedures were performed in accordance with the NIH guidelines for the care and use of laboratory animals (NIH Publication no. 85–23 Rev. 1985) and approved by the Jiangsu Administration of Experimental Animals with the approval number IACUC-2306006.

IDEAL-$NK_{PT/Cy5/BHQ3}$ cells were prepared with BHQ3 labelled IL-21 APs and Cy5 labelled poly-DNA1. BHQ3 was labelled on L1 strand for IL-21 APs, and Cy5 was labelled on P1a strand for poly-DNA1. Cy5 fluorescence was quenched for IDEAL-$NK_{PT/Cy5/BHQ3}$ cells upon hybridization of L1 and poly-DNA1. Disulfide bonds were also modified on L1 strand to demonstrate GSH responsive DNA scaffold decapsulation. The mice were intravenously injected with IDEAL-$NK_{PT/Cy5/BHQ3}$ cells (100 μL, 1×10^7 cells), and were sacrificed after 24 h. The tumor, heart, liver, spleen, lungs, and kidneys were dissected and collected for imaging analysis. DOX fluorescence was collected at 580 nm to indicate the distribution and infiltration of IDEAL-NK cells. Cy5 fluorescence was collected in vivo at 700 nm to indicate the release of NK cells from DNA scaffold.

IL-NK_{DID} cells, NK_{DID}-$PLGA_{drugs}$ cells and $IDEAL_{PT}$-NK_{DID} were stained with DID (1 μM) in pre-warmed serum-free medium at 37 °C for 20 min, gently inverting the tube every 5–10 min. After incubation, added PBS and centrifuged at 1000 rpm for 5 min, and then discarded the supernatant. Repeated this washing step 3 times for subsequent use.

2.16. In vivo therapeutic effect evaluation

A549 tumor bearing mice were randomly divided into five groups ($n = 5$), intravenously injected with 1×10^7 IL-NK cells, NK- $PLGA_{drugs}$ cells, $IDEAL_{PT}$-NK cells, $PLGA_{drugs}$ NPs (2 mg/kg, 100 μL) and saline (100 μL) respectively. The administration was performed on day 1, day 6 and day 18 respectively. The body weight of the mice as well as the tumor size were measured every 3 days. All mice were sacrificed on day 28 and the tumors were dissected for TUNEL and H&E staining to assess the level of apoptosis at tumor site. In addition, major organs such as the heart, liver, spleen, lungs, and kidneys were dissected and collected for histopathological analysis to evaluate the therapeutic safety. Tissue imaging was also performed on dissected tumor sites and major organs to verify the accumulation of administrated $IDEAL_{PT}$-NK cells.

To evaluate in vivo adoptive NK cells activation in local tumors, mice were sacrificed at the end of different treatments, and their blood and tumors were collected. The expression levels of IL-2, GzmB and TNF-α in the mouse serum were measured with ELISA kits, respectively.

3. Results and discussion

3.1. Preparation of IL-NK cells and characterizations of reducing environment responsive IL-21 NPs decompose

IL-21 nanoparticles (IL-21 NPs) were synthesized by crosslinking IL-21 protein with GSH-responsive small molecule cross-linker NHS-SS-NHS (Fig. S1 A, synthesis), which demonstrated a band with obvious lower mobility compared with cytokine IL-21 monomer band on SDS-PAGE gel (Fig. S1B, lane 1,2). The as-obtained IL-21 NPs were sized in 25 ± 3.3 nm in TEM (Fig. 1A) with hydrate diameter of ~34.7 nm (Fig. S1C) and zeta potential of −2.1 mV (Fig. 1B, IL-21 NPs).

CD45 antibody and NH_2-functionalized DNA strand L1 were subsequently conjugated to residual NHS groups on the surface of IL-21 NPs via amide reaction to prepare IL-21 anchoring nanoparticles (IL-21 APs) (Fig. 1C, IL-21 APs), which decreased zeta potential to −7.2 mV (Fig. 1B, IL-21 APs). IL-21 APs was incubated with NK-92MI cells to prepare IL-NK cells. Anti-CD45 recognized CD45 receptors that highly expressed on NK-92MI cell membrane, while DNA strand L1 acted as anchor to hybrid with poly-DNA1 for the subsequent construction of DNA scaffold on cell membrane. Cy5 labelled IL-21 APs (IL-21_{Cy5} APs) treated NK-92MI cells (IL_{Cy5}-NK cells) showed strong Cy5 fluorescence surrounding cell membrane (Fig. 1D, IL_{Cy5}-NK), indicating efficient attachment of IL-21 APs on NK-92MI cells. On the contrary, incubating IL-21_{Cy5} NPs that in the absence of anti-CD45 with NK cells didn't demonstrate membrane Cy5 fluorescence (Fig. 1D, NK + IL-21 NPs).

IL-21 APs decompose due to the cleavage of disulphide bonds in reducing environment such as glutathione (GSH)) (Fig. 1C, decompose), which not only liberated NK cells from DNA scaffold, but also enhanced its activity by the released cytokine IL-21 monomer. To mimic reducing environment, 10 mM GSH was incubated with IL-21 NPs, and resulted in higher mobility band at the corresponding position of cytokine IL-21 monomer with the disappearance of IL-21 NPs band (Fig. S1A, decompose; Fig. S1B, lane 4), indicating the successful decompose of IL-21 NPs with efficient release of cytokine IL-21. Time corresponding release of IL-21 from IL-21 APs upon GSH treatment was further evaluated by dialyzing the reaction mixture, the released monomer cytokine IL-21 was collected outside dialysis bag and quantified by ELISA, which gradually increased in the beginning 4 days of treatment and saturated at approximately 85 % within 7 days (Fig. S2A, IL-21 APs + GSH). On the contrary, IL-21 APs was stable in the absence of GSH treatment, and the release percentage remained below 15 % over 7 days (Fig. S2A, IL-21 APs).

To further verify release of IL-21 from IL-NK cells, IL_{Cy5}-NK cells that prepared with IL-21_{Cy5} APs were cultured in GSH-containing 1640 medium for 24 h. It demonstrated decrease of Cy5 fluorescence from IL_{Cy5}-NK cell membrane (Fig. 1D, IL_{Cy5}-NK + GSH), which was accompanied by the increase of Cy5 fluorescence from cell culture medium supernatant (Fig. S2B, GSH(+)). On the contrary, IL_{Cy5}-NK cells demonstrated stable Cy5 fluorescence surrounding cell membrane during 24 h culturing in the absence of GSH (Fig. S3). The cell culture medium supernatant barely showed Cy5 fluorescence either (Fig. S2B, GSH(−)). The released monomer cytokine IL-21 was quantified from supernatant of cell culture medium via ELISA, and divided by centrifugation to obtain IL-21 release percentage of ~56 % in the presence of GSH and ~ 9 % in the absence of GSH (Fig. S2C). These results confirmed the efficiency of IL-21 APs decompose in reducing environment, which guaranteed successful liberation of NK-92MI cells.

3.2. Preparation and characterizations of DNA-NK cells

As the construction components for DNA scaffold, poly-DNA1 was

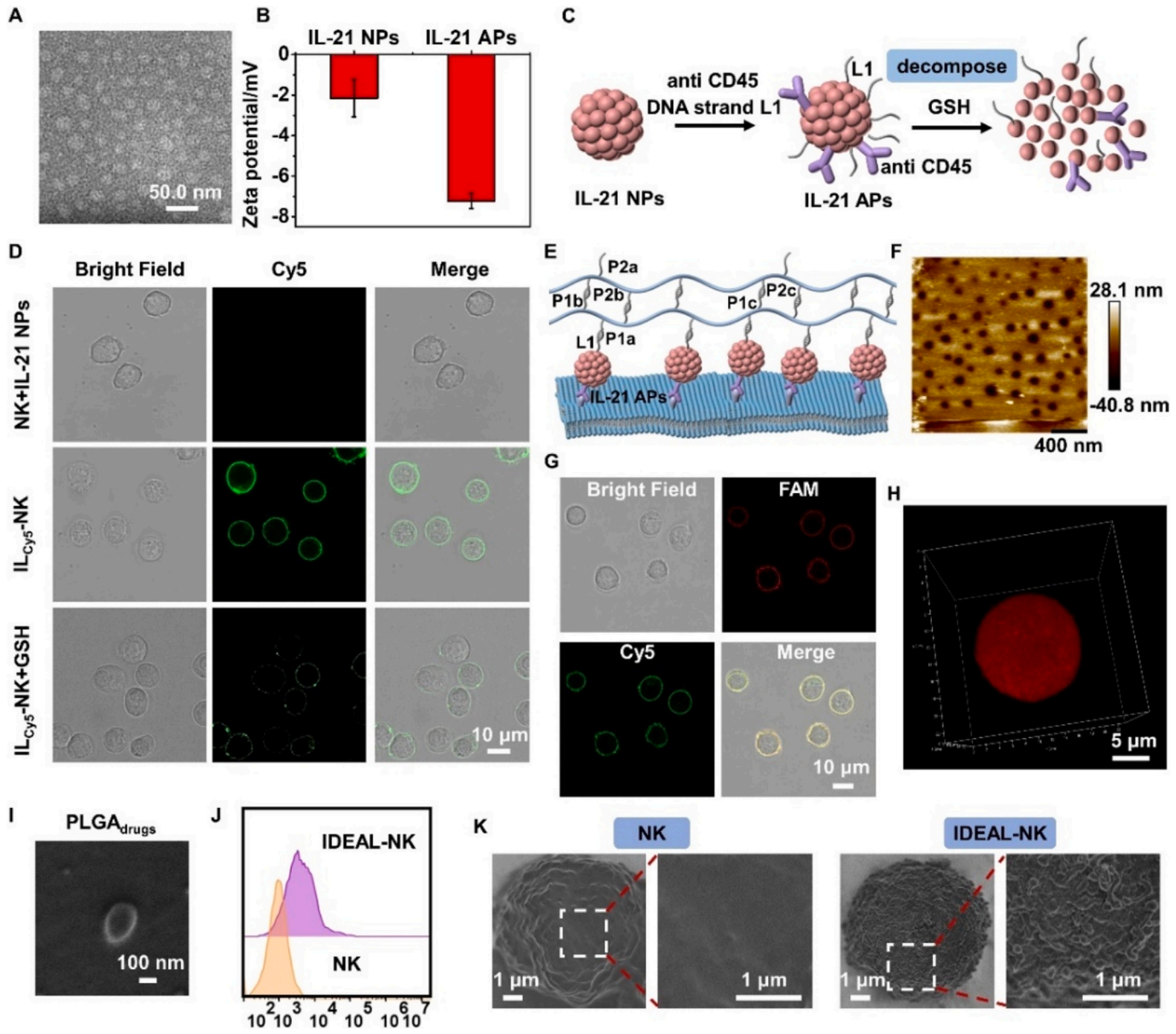

Fig. 1. Preparation and characterizations of IDEAL-NK cells. (A) Transmission electron microscopy morphological determination of IL-21 NPs. (B) The zeta potential analysis of IL-21 NPs and IL-21 APs. (C) Schematic illustration of IL-21 APs preparation and glutathione responsive decompose. (D) Confocal laser scanning microscopy (CLSM) images of NK cells incubated with IL-21 NPs (NK + IL-21 NPs), IL-21 APs (IL$_{Cy5}$-NK), and IL-21 APs incubated NK cells with glutathione treatment (IL$_{Cy5}$-NK + GSH). (E) Schematic illustration of DNA scaffold assembly on IL-NK cell membrane. (F) Atomic force microscopy characterization of DNA scaffold. (G) Confocal laser scanning microscopy images of DNA$_{FAM/Cy5}$-NK cells. (H) Three dimensions-stack image of DNA$_{Cy5}$-NK cells. (I) Transmission electron microscopy image of PLGA$_{drugs}$ NPs. (J) Flow cytometry analysis and (K) Scanning electron microscopy image of NK cells and IDEAL-NK cells.

synthesized by copolymerizing acrylamide residues with the acrydite-modified DNA strands P1a, P1b, P1c (Fig. S4A), and poly-DNA2 was synthesized by copolymerizing acrylamide residues with the acrydite-modified DNA strands P2a, P2b, P2c (Fig. S4B). The successful generations of poly-DNA were confirmed by PAGE. P1a, P1b, P1c (Fig. S5A, lane1, lane2, lane3) and P2a, P2b, P2c showed a clear single band with high mobility respectively, while the bands for poly-DNA1 (Fig. S5A, lane4) and poly-DNA2 (Fig. S5A, lane8) demonstrated much lower mobilities. In addition, the fourier transform infrared spectroscopy (FTIR) spectrum of P1a/P1b/P1c/acrylamide mixture showed C═O stretching vibration characterization peak at around 1666 cm^{-1} and C═C stretching vibration characteristic peak at 1611 cm^{-1} (Fig. S5B, a), while the C═C stretching vibration characteristic peak was disappeared for poly-DNA1 (Fig. S5B, b), indicating successful polymerization of DNA strands and generation of poly-DNA strands.

P1a in poly-DNA1 has complimentary sequence with L1 strand from IL-21 APs, P1b and P1c in poly-DNA1 have complimentary sequences with P2b and P2c in poly-DNA2 respectively. Poly-DNA1 and poly-DNA2 were sequentially hybridized to IL-NK cells to assemble DNA scaffold on NK cell membrane (Fig. 1E). The sequence complimentary of DNA strands were verified via PAGE analysis, which showed a new single band with lower mobility both for the mixture of L1 with P1a, P1b with P2b, and P1c with P2c (Fig. S6, lane 3, lane 6, lane 9). The specific hybridization of DNA strands guaranteed the efficient construction of DNA scaffold on NK cell membrane. The microscopic morphology of constructed DNA scaffold was characterized by atomic force microscope (AFM), which showed typical network structure with microscale pores around ~100 nm (Fig. 1F).

To visualize the construction of DNA scaffold on NK cell membrane, FAM-labelled P1b and Cy5-labelled P2c were used to prepare poly-

$DNA1_{FAM}$ and poly-$DNA2_{Cy5}$, respectively. The as-obtained $DNA_{FAM/Cy5}$-NK cells showed good co-localization of FAM and Cy5 fluorescence on cell membrane (Fig. 1G), indicating efficient encapsulation of DNA scaffold on NK cell membrane. 2D Z stacking imaging and 3D reconstruction also showed uniform and sufficient coverage of NK cells with Cy5 fluorescence, indicating the efficient density for as-obtained DNA scaffold and corresponding integral wrapping of NK cells (Fig. 1H). The as-obtained DNA scaffold on cell membrane provided sufficient binding positions for subsequent $PLGA_{drugs}$ NPs anchoring, while effectively protected NK cells from drug toxicity, which would make the as-obtained DNA-NK cell eligible drug carrier while well remained its immune activity.

3.3. Preparation and characterizations of IDEAL-NK cells

$PLGA_{drugs}$ NPs were prepared by emulsion method and loaded with DOX for chemotherapy and verapamil to stimulate GSH efflux from tumor cell [47,48], which not only sensitized tumor cells to chemotherapy [49], but also raised reducing condition in microenvironment to promote IL-21 APs decompose. $PLGA_{drugs}$ NPs were sized in approximate 230 nm (Fig. 1I) with hydrate diameter of ~238 nm (Fig. S7A) and zeta potential of −6.5 mV (Fig. S7B, $PLGA_{drugs}$ NPs). DNA strand N1 was functionalized with NH_2 group, and was modified to $PLGA_{drugs}$ NPs via a ROS responsive linker NHS-TK-NHS. The as-obtained $PLGA_{drugs}$-N1 NPs demonstrated hydrate diameter of ~281 nm (Fig. S7C) and zeta potential of −14.6 mV (Fig. S7B, $PLGA_{drugs}$-N1 NPs), much lower than $PLGA_{drugs}$ NPs due to the negative charge of DNA strand N1.

The as-obtained $PLGA_{drugs}$-N1 NPs was anchored to DNA-NK cell via N1/P2a hybridization to obtain IDEAL-NK cells (Fig. S8A). The hybridization of complementary DNA strands P2a and N1 was verified with PAGE analysis, their mixture showed a single band with lower mobility compared with P2a or N1 strand (Fig. S6, lane 12). DOX fluorescence was observed with flow cytometry to confirm the anchoring of $PLGA_{drugs}$ NPs on IDEAL-NK cell membrane, which demonstrated obviously increased fluorescence intensity compared with untreated NK cells (Fig. 1J). Confocal fluorescence microscopy also demonstrated clear fluorescence in the region of 580–620 nm around cell membrane (Fig. S8B). SEM images showed much rougher surface for IDEAL-NK cells with randomly distributed particles on cell membrane compared with untreated NK cells (Fig. 1K), confirmed the efficient attachment of $PLGA_{drugs}$ NPs on IDEAL-NK cell membrane. To calculate the loading capacity of $PLGA_{drugs}$ NPs, it was incubated with IDEAL-NK cells, and the un-anchored $PLGA_{drugs}$ NPs that remain in supernatant were collected by centrifugation and quantified by measuring DOX fluorescence intensity and comparing with $PLGA_{drugs}$ NPs calibration curve to obtain $PLGA_{drugs}$ NPs loading capacity as ~68 % (Fig. S9A), and the corresponding loading amount was 39.7 $\mu g/10^7$ cells. To calculate the loading amount of IL-21 Aps on cell membrane, IL-21 APs were labelled with Cy5 (IL-21_{Cy5} APs) and the Cy5 fluorescence was quantified using the same method. The loading amount of IL - 21 APs was determined to be 0.94 $\mu g/10^7$ cells (Fig. S9B). Cytotoxicity of DNA scaffold was evaluated via MTT assay, IL-NK cells, DNA-NK cells and IDEAL-NK cells all showed over 90 % of cell viabilities (Fig. S9C).

The encapsulation of DNA scaffold around NK cells effectively enhanced drug loading capacity, while efficiently protected NK cells viability from chemical toxic drugs. The encapsulation density of DNA scaffold on NK cell was optimized to evaluate its protection capability against loaded drugs. The concentrations of poly-DNAs, as the DNA scaffold components, were set as 0.5 μM and 5 μM. Untreated NK cells and NK-$PLGA_{drugs}$ cells were set as positive control and negative control respectively. NK-$PLGA_{drugs}$ cells were prepared by directly hybridizing $PLGA_{drugs}$ NPs to IL'-NK cells in the absence of DNA scaffold encapsulation. IL'-NK cells were prepared with DNA strand L1' instead of L1, where L1' could hybridize with N1 to anchor $PLGA_{drugs}$ NPs on cell membrane. DOX fluorescence was observed via confocal imaging to compare the loading amounts of $PLGA_{drugs}$ NPs on IDEAL-NK cells, which showed intense and uniformly distributed fluorescence surrounding cell membrane for IDEAL-NK cells that fabricated with higher DNA scaffold density (Fig. 2A, IDEAL-NK, 5 μM), indicating the sufficient loading of $PLGA_{drugs}$ NPs on cell membrane without internalization. On the contrary, IDEAL-NK cells fabricated with lower DNA scaffold density showed some intracellular DOX fluorescence, indicating internalization of $PLGA_{drugs}$ NPs to some extent (Fig. 2A, IDEAL-NK, 0.5 μM). Obvious internalization of $PLGA_{drugs}$ NPs was observed for NK-$PLGA_{drugs}$ cells (Fig. 2A, NK-$PLGA_{drugs}$). Using primary NK cells instead of NK-92MI cells, we prepared IDEAL-$NK_{primary}$ cells with different DNA densities, and similar $PLGA_{drugs}$ NPs distribution trends were observed (Fig. S10). These results indicated higher DNA scaffold encapsulation density provided satisfactory protection of NK cells from $PLGA_{drugs}$ NPs. The viability of IDEAL-NK cell was further evaluated via MTT assay and flow cytometry to confirm the protection capability of DNA scaffold. Higher density of DNA scaffold encapsulation maintained over 90 % of cell viability upon 24 h culture (Fig. S11A, IDEAL-NK, 5 μM; IDEAL-NK, 10 μM; IDEAL-NK, 20 μM), while lower DNA scaffold density encapsulation resulted in ~70 % of cell viability (Fig. S11A, IDEAL-NK, 0.5 μM), and NK-$PLGA_{drugs}$ showed ~50 % of cell death (Fig. S11A, NK-$PLGA_{drugs}$). Using primary NK cells instead of NK-92MI cells, we observed similar cell viability change (Fig. S11B). Flow cytometry demonstrated similar tendency, IDEAL-NK cells with high encapsulation density, low encapsulation density, and NK-$PLGA_{drugs}$ cells showed apoptosis rates of 7.3 %, 29.0 %, 49.1 % respectively (Fig. 2B). These results confirmed the capability of DNA scaffold as an efficient and safe encapsulation layer for drugs loading and NK cells activity protection.

Tumor and inflammatory tissues release stroma-derived factor-1 (SDF-1), a chemokine that recognized by C-X-C motif chemokine receptor 4 (CXCR4) on immune cells membrane to drive its active movement toward injury sites [50]. To evaluate the influence of DNA scaffold encapsulation on NK cells communication with surrounding environment and corresponding tumor homing capability, FITC labelled SDF-1 (FITC-SDF-1) were incubated with IDEAL$_{Cy5}$-NK cells that prepared with different encapsulation densities of DNA_{Cy5}-scaffold and NK-$PLGA_{drugs}$ cells, which showed similar FITC intensities at cell membrance for all the treated cells and good overlaps with membrane Cy5 fluorescence (Fig. S12). These results indicated good chemokine permeability for as-obtained DNA scaffold on NK cell membrane, and confirmed DNA scaffold would not affect intercellular communication for IDEAL-NK cells.

Transwell experiments were further performed to evaluate the migration capability of IDEAL-NK cells. Two-dimensional cellular models were established to mimic the process of NK cells approaching tumor site. IDEAL-NK cells with high DNA encapsulation density and low DNA encapsulation density, as well as NK-$PLGA_{drugs}$ cells were seeded in the upper chamber respectively, A549 cells were seeded in the lower chamber which secreted chemotactic including SDF-1 as stimulators to induce directed migration of immune cells. IDEAL-NK cells and NK-$PLGA_{drugs}$ cells were all stained with CFSE dye for location indication, and the cells that migrated into the lower chamber were observed via confocal microscopy and counted via cell counting plates for quantification after 24 h incubation, the migration ratios of IDEAL-NK cells with high DNA encapsulation density, IDEAL-NK cells with low DNA encapsulation density, and NK-$PLGA_{drugs}$ cells were ~ 90 %, ~77 %, and ~ 50 %, respectively (Fig. 2C, S13). DNA-scaffold encapsulation didn't affect targeting capability of NK cells, therefore all the lower chambers were occupied by IDEAL-NK cells and NK-$PLGA_{drugs}$ cells obviously. High DNA encapsulation density provided satisfactory protection of NK cell activity, therefore demonstrated most efficient transmigration capability with largest number of transmitted cells in the lower chamber (Fig. 2C, S13, IDEAL-NK, 5 μM).

3.4. In vitro verification of $PLGA_{drugs}$ NPs release and chemotherapy

As endogenous stimuli, redox and reducing conditions in tumor

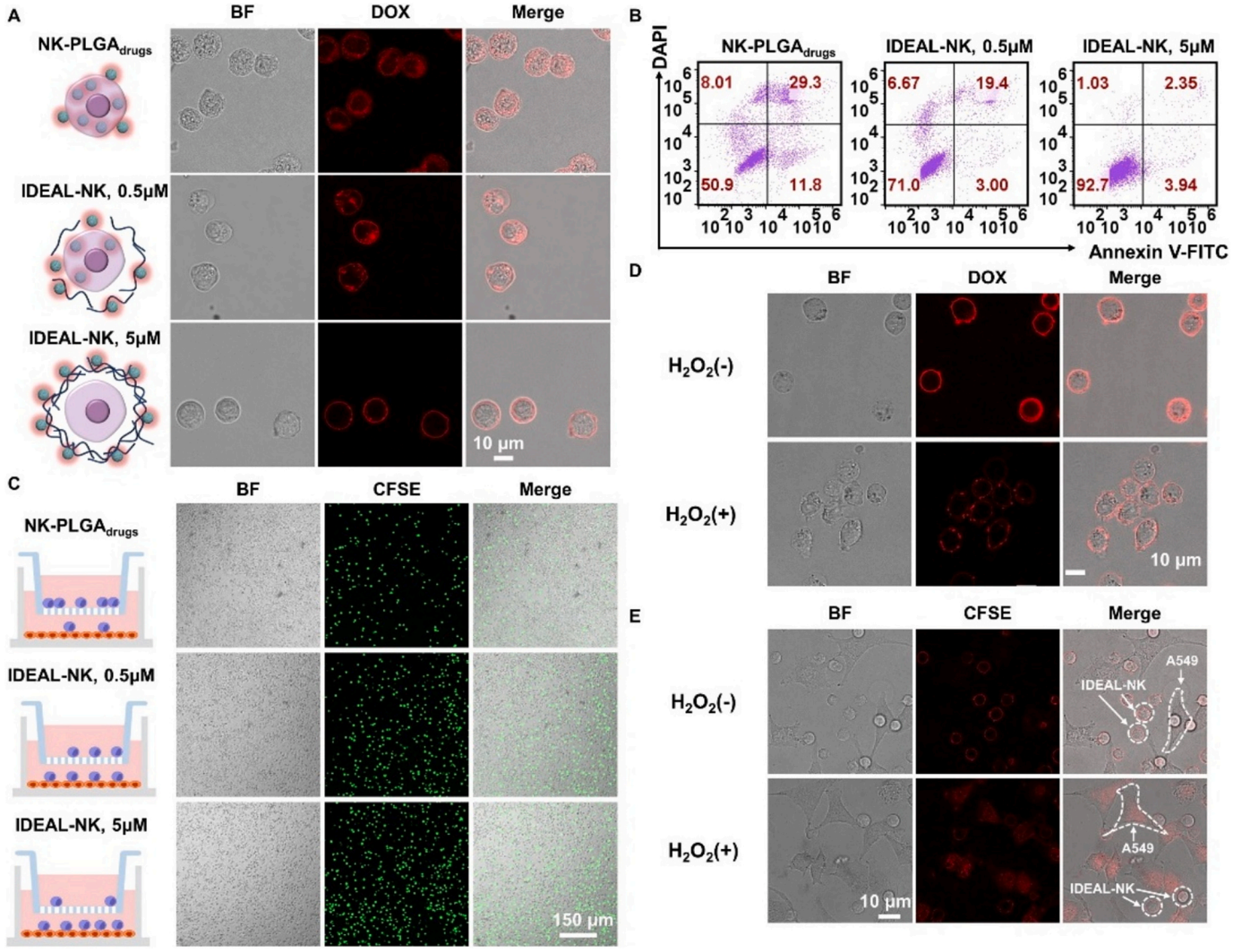

Fig. 2. Characterization of IDEAL-NK cells and H_2O_2 responsive chemotherapy. (A) Confocal laser scanning microscopy, (B) flow cytometry based live/dead characterization, and (C) migration characterization of IDEAL-NK cells prepared with different encapsulation densities of DNA scaffold and NK-PLGA$_{drugs}$ cells that have PLGA$_{drugs}$ NPs directly anchored on NK cell membrane. (D) Confocal laser scanning microscopy of IDEAL-NK cells and (E) localization of PLGA$_{drugs}$ NPs in a mixed culture system of IDEAL-NK cells and A549 cells before (H_2O_2(−)) and after (H_2O_2(+)) H_2O_2 treatment.

microenvironment were programmed for sequent release of PLGA$_{drugs}$ NPs and liberation of NK cells. TK linker that connected PLGA$_{drugs}$ NPs to DNA scaffold was cleaved in response to ROS in the tumor microenvironment, enabling tumor site-responsive release of PLGA$_{drugs}$ NPs (Scheme 1B, PLGA$_{drugs}$ NPs release). When PLGA$_{drugs}$ NPs is released from IDEAL-NK cells, DNA scaffold should still remain intact to protect NK cells from drug toxicity. Due to the efficient loading of PLGA$_{drugs}$ NPs, IDEAL-NK cells showed clear DOX outline around cell membrane before H_2O_2 treatment (Fig. 2D, H_2O_2(−)). H_2O_2 treatment resulted in substantial decrease of DOX fluorescence from cell membrane, which indicated efficient detachment of PLGA$_{drugs}$ NPs from IDEAL-NK cells (Fig. 2D, H_2O_2(+)). Dense packing of DNA scaffold effectively prevented the endocytosis of liberated PLGA$_{drugs}$ NPs into NK cell, therefore DOX fluorescence was barely observed from NK cell intracellularly. On the contrary, NK-PLGA$_{drugs}$ cell that in the absence of DNA scaffold protection showed blurry DOX fluorescence boundary at cell membrane before H_2O_2 treatment due to the partial endocytosis of attached PLGA$_{drugs}$ NPs (Fig. S14, H_2O_2(−)). H_2O_2 treatment of NK-PLGA$_{drugs}$ cell resulted in obvious intracellular DOX fluorescence due to the endocytosis of released PLGA$_{drugs}$ NPs (Fig. S14, H_2O_2(+)).

ROS responsive PLGA$_{drugs}$ NPs release and A549 cell selective toxicity were further evaluated in IDEAL-NK cells and A549 cells co-culture medium. A549 cells and IDEAL-NK cells were discriminated by their different morphologies in bright field image. A549 cell has attachment tendency to cell culture plate, and demonstrates a tentacle morphology. NK cell has suspension growth character, and demonstrates round morphology. The location of PLGA$_{drugs}$ NPs was indicated by DOX fluorescence. IDELA-NK cells and A549 cells co-cultured medium in the absence of H_2O_2 treatment demonstrated clear DOX fluorescence from NK cell membrane, while little intracellular fluorescence was observed for A549 cells (Fig. 2E, H_2O_2(−)). When treated with H_2O_2, PLGA$_{drugs}$ NPs was liberated from IDEAL-NK cells and selectively endocytosed by A549 cells, which showed obvious intracellular DOX fluorescence from A549 cells accompanied by disappearance of DOX fluorescence from IDEAL-NK cell membrane (Fig. 2E, H_2O_2(+)). The as-obtained DNA-NK cells barely showed intracellular DOX fluorescence, further confirmed the satisfactory protection from DNA scaffold. On the contrary, when treated NK-PLGA$_{drugs}$ cell and A549 cells co-culture media with H_2O_2, DOX fluorescence was observed both from A549 cells and NK cells due to the lack of DNA scaffold protection for NK-PLGA$_{drugs}$ cells (Fig. S15, H_2O_2(+)).

To evaluate the chemotherapeutic effect of IDEAL-NK cells, NK cell with non-degradable DNA scaffold was prepared by replacing degradable IL-21 APs with nondegradable IL-21 APs (IL-21$_{non}$ APs) which

crosslinked IL-21 with NHS-PEG$_2$-NHS. The as-obtained Non-degraded IL-21 and Drug Equipped AcryL-DNA scaffold framed NK cells (NIDEAL-NK) couldn't respond to reduction environment to disassemble DNA scaffold for NK cell release, therefore suppressed the immunoactivity of NK cells and only demonstrated chemotoxicity of PLGA$_{drugs}$ NPs. When co-culturing NIDEAL-NK cells with A549 cells, it resulted in over 90 % and ~ 59 % of cell viability for A549 cells in the absence ($H_2O_2(-)$) and presence ($H_2O_2(+)$) of H_2O_2 treatment respectively (Fig. S16), indicating the chemotherapeutic effect of released PLGA$_{drugs}$ NPs.

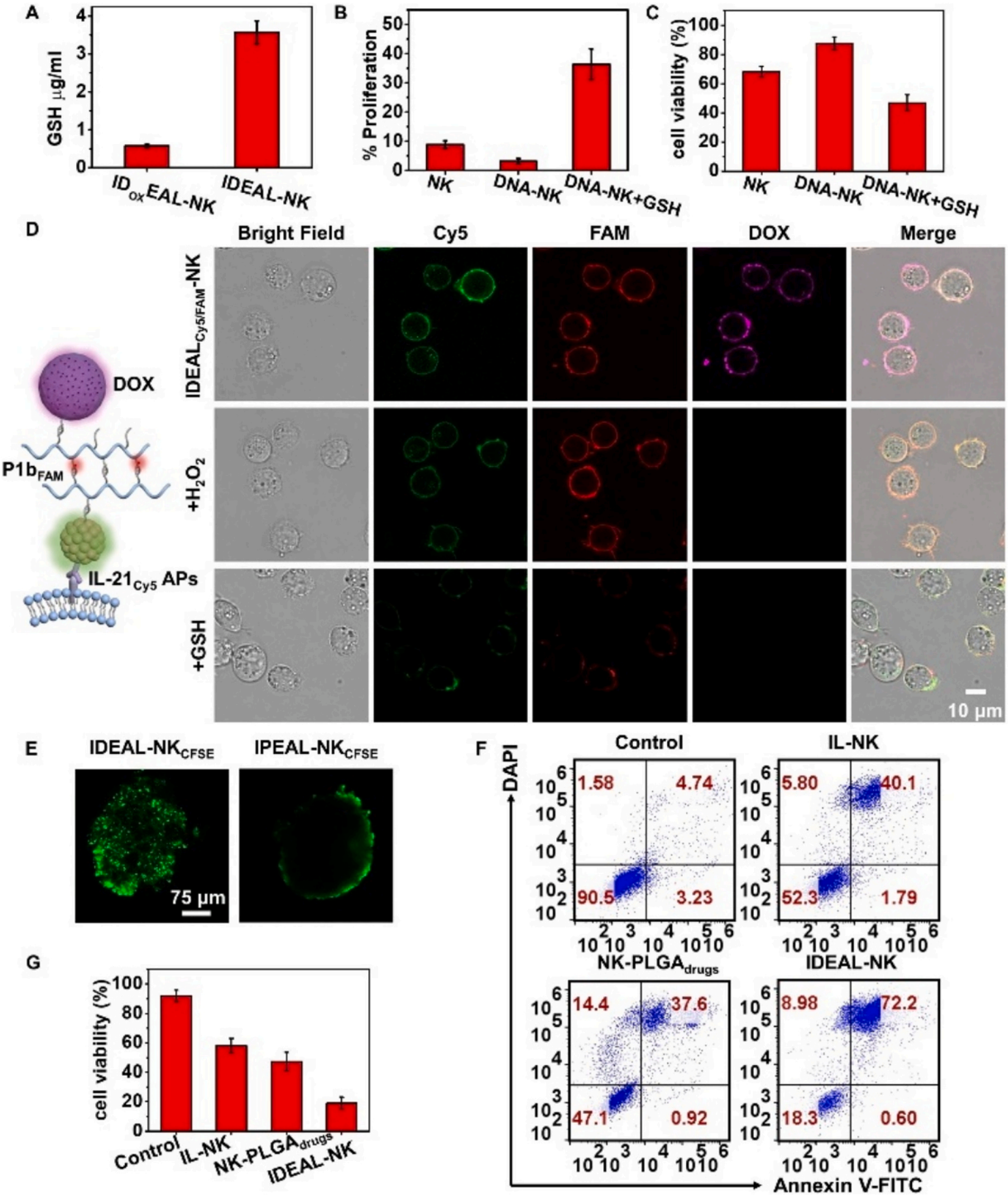

Fig. 3. Characterization of tumor cell killing capacity of IDEAL-NK cells. (A) Enzyme - linked immunosorbent assay of glutathione efflux from A549 cells after incubation with IDEAL-NK cells and ID$_{OX}$EAL-NK cells that prepared with PLGA$_{DOX}$ NPs that only loaded with DOX but not verapamil. (B) Proliferation of NK cells, DNA-NK cells, and DNA-NK cells in presence of glutathione (DNA-NK + GSH) (n = 3). (C) MTT cell viability assay of A549 cells incubated with NK cells, DNA-NK cells, and DNA-NK cells in presence of glutathione (DNA-NK + GSH) (n = 3). (D) (E) Penetration of IDEAL-NK$_{CFSE}$ cells and IPEAL-NK$_{CFSE}$ cells into A549 tumor spheroids (MTSs). Green fluorescence represents NK cells. (F) Flow cytometry assay and (G) MTT cell viability assay of A549 cells incubated with IL-NK cells, NK-PLGA$_{drugs}$ cells and IDEAL-NK cells. (For interpretation of the references to colour in this figure legend, the reader is referred to the web version of this article.)

3.5. In vitro verification of NK cell decapsulation and killing capability

Verapamil, a drug that interacts with multidrug resistance protein 1 (MPR1) and induces rapid and massive efflux of cellular GSH [51], was also loaded to $PLGA_{drugs}$ NPs, which would enhance GSH level in tumor microenvironment to decompose IL-21 APs with the decapsulation of NK cells. When co-culturing IDEAL-NK cells with A549 cells, A549 cells generated H_2O_2 and secreted it to the extracellular space [52]. $PLGA_{drugs}$ NPs were correspondingly released and endocytosed by A549 cells to trigger efflux of GSH to co-culture medium, which turned the co-culture system to reduction microenvironment. As control, the $ID_{ox}EAL$-NK cells were prepared with $PLGA_{DOX}$ NPs that only loaded DOX for chemotherapy but not verapamil for stimulating GSH efflux instead of $PLGA_{drugs}$ NPs. IDEAL-NK cells and $ID_{ox}EAL$-NK cells were incubated with A549 cells respectively, and the amount of effluxed GSH in culture medium was evaluated via ELISA kit. IDEAL-NK cells treated group showed a 7-fold elevation of extracellular GSH compared with $ID_{ox}EAL$-NK cells treated group (Fig. 3A). These results indicated $PLGA_{drugs}$ NPs release effectively enhanced reducing condition in tumor microenvironment, which subsequently guaranteed efficient IL-21 APs decompose and corresponding NK cell release.

The effluxed GSH penetrates through DNA scaffold to decompose IL-21 APs and disassemble DNA scaffold. The in situ generation of cytokine IL-21 contributes to NK cell expansion. To evaluate the contribution effect, DNA-NK cells were incubated in culture medium with GSH, and the cell proliferation rate was compared with DNA-NK cells in the absence of GSH addition and untreated NK cells. DNA-NK cells in the absence of GSH showed proliferation rate of 3.2 % (Fig. 3B, DNA-NK), which was lower than that of untreated NK cells (8.9 %) (Fig. 3B, NK) due to the physical constraint of DNA scaffold, while the proliferation rate for DNA-NK cells in presence of GSH was enhanced to 36.4 % (Fig. 3B, DNA-NK + GSH). In addition to proliferation, cytokine IL-21 generation also enhanced cancer cell killing capability of NK cells. The contribution effect was evaluated via MTT assays. When co-cultured DNA-NK cells and A549 cells in presence of GSH, it resulted in lowest viability of 36.9 % for A549 cells (Fig. 3C, DNA-NK + GSH), while untreated NK cells resulted in 65.2 % of cell viability for co-cultured A549 cells (Fig. 3C, NK). These results indicated that the in situ decapsulation of NK cell with IL-21 cytokine release effectively enhanced its tumor cell killing capability. Considering the limitation of DNA scaffold to NK cell proliferation and intercellular contact, co-culturing DNA-NK cells with A549 cells in the absence of GSH resulted in 85.7 % of A549 cell viability (Fig. 3C, DNA-NK).

3.6. Programmable release of $PLGA_{drugs}$ NPs and disassembly of DNA scaffold to boost adoptive NK cell therapy

Programming the timing for $PLGA_{drugs}$ NPs release and NK cell liberation is important to boost the therapeutic effect of IDEAL-NK cells. To visualize the programmable sequential release of $PLGA_{drugs}$ NPs, detachment of DNA scaffold, and liberation of NK cells, $IL\text{-}21_{Cy5}$ APs were labelled with fluorescent dye Cy5. $P1b_{FAM}$, as the component for DNA scaffold, was labelled with fluorescent dye FAM. The fluorescence of Cy5, FAM and DOX were imaged under confocal microscopy, which co-localized very well for $IDEAL_{Cy5/FAM}$-NK cells (Fig. 3D, $IDEAL_{Cy5/FAM}$-NK). To mimic tumor microenvironment, $IDEAL_{Cy5/FAM}$-NK cells were subsequently incubated with H_2O_2, which showed a significant decrease of DOX fluorescence from cell membrane, indicating the efficient detachment of $PLGA_{drugs}$ NPs (Fig. 3D, $+H_2O_2$). FAM fluorescence and Cy5 fluorescence were still co-localized well on cell membrane for the as-obtained $DNA_{Cy5/FAM}$-NK cells (Fig. 3D, $+H_2O_2$), indicating the DNA scaffold remained stable on NK cell membrane during $PLGA_{drugs}$ NPs release process. To mimic the enhanced reducing condition after $PLGA_{drugs}$ NPs release, the as-obtained $DNA_{Cy5/FAM}$-NK cells were continuously incubated with GSH, which intensively reduced both Cy5 and FAM fluorescence intensities on cell membrane for the as-obtained NK cell (Fig. 3D, +GSH), indicating the sufficient detachment of DNA scaffold and liberation of NK cells. Using primary NK cells instead of NK-92MI cells, we prepared $IDEAL_{Cy5/FAM}\text{-}NK_{primary}$ cells. Then these cells were sequentially incubated with H_2O_2 and GSH, and demonstrated similar trends for the disappearance of DOX fluorescence and FAM/Cy5 fluorescence as those for NK-92MI cells, indicating the successful liberation of primary NK cells from DNA scaffold (Fig. S17).

The preceding execution of chemotherapy from $PLGA_{drugs}$ NPs resulted in apoptosis of tumor cells, loosed the tumor structure, and reprogrammed a more favorable microenvironment for the engraftment and infiltration of adoptive NK cells [53]. Three-dimensional (3D) multicellular A549 tumor spheroids (MTSs) model was set up to evaluate the tumor infiltration capability of adoptive NK cells. $IDEAL\text{-}NK_{CFSE}$ cells were labelled with CFSE dye to indicate its tissue infiltration via confocal z-stack imaging. The control group was set by incubating A549 MTSs model with IL-21 APs and PLGA NPs equipped acryl-DNA scaffold framed NK_{CFSE} cells ($IPEAL\text{-}NK_{CFSE}$), which didn't have drugs loading in PLGA. CFSE fluorescence from A549 MTSs section at the same height from the bottom was compared. CFSE fluorescence for $IDEAL\text{-}NK_{CFSE}$ cell culturing group was spread almost all over the section (Fig. 3E, $IDEAL\text{-}NK_{CFSE}$), indicating good penetration capability of $IDEAL\text{-}NK_{CFSE}$ cells. On the contrary, $IPEAL\text{-}NK_{CFSE}$ cells culturing group only showed CFSE fluorescence distributed at the edge of the section (Fig. 3E, $IPEAL\text{-}NK_{CFSE}$), indicating NK cells only stayed in the peripheral area of the MTSs. These results confirmed that chemotherapy effectively facilitated the infiltration of NK cells at the tumor site.

The contribution of preceding chemotherapy to IDEAL-NK cell killing capability was evaluated by measuring the apoptosis of co-cultured A549 cells via flow cytometry. Due to the combination therapeutic effects of chemotherapy from $PLGA_{drugs}$ NPs and immune-killing from NK cells, A549 cells that co-cultured with IDEAL-NK cells showed apoptosis rate of 81.7 % (Fig. 3F, IDEAL-NK). Control group was set by incubating A549 cells with IL-NK cells which only anchoring IL-21 APs to NK cell membrane in the absence.

of DNA scaffold encapsulation and $PLGA_{drugs}$ loading. The stimulation from A549 cells improved reducibility of NK cells membrane [54], which release IL-21 from IL-21 APs to enhance NK cell killing capability. IL-NK cells only showed immune therapeutic effect to co-cultured A549 cells with 47.7 % of cell apoptosis (Fig. 3F, IL-NK). These results indicated the contribution of preceding chemotherapy to immunotherapy efficiency of NK cells. $NK\text{-}PLGA_{drugs}$ cells that have $PLGA_{drugs}$ NPs directly anchored on cell membrane without DNA scaffold encapsulation were set as another control group, which resulted in 52.9 % of A549 cell apoptosis (Fig. 3F, $NK\text{-}PLGA_{drugs}$). Due to the lack of DNA scaffold protection, NK cell activity was impaired by endocytosis of $PLGA_{drugs}$ NPs, therefore limited the therapeutic effect of chemotherapy combined immunotherapy for $NK\text{-}PLGA_{drugs}$ cells. Using primary NK cells instead of NK-92MI cells to repeat this experiment, similar A549 apoptosis tendency was observed (Fig. S18). These results further confirmed the programmable release of $PLGA_{drugs}$ NPs and liberation of NK cells is important for boosting adoptive cell therapy. MTT assay demonstrated similar tendency as flow cytometry result. A549 cells that treated with IDEAL-NK cells showed lowest cell viability of ~20 %, while A549 cells that treated with IL-NK cells or $NK\text{-}PLGA_{drugs}$ cells showed cell viability of ~50 % and ~ 45 % respectively (Fig. 3G).

3.7. In vivo verification of IDEAL-NK cells therapeutic efficiency

Phosphorothioate-modified DNA strands $L1_{PT}$, $P1a_{PT}$, $P1b_{PT}$, $P1c_{PT}$, $P2a_{PT}$, $P2b_{PT}$, $P2c_{PT}$, and $N1_{PT}$ were used as components to synthesize IDEAL-NK cells to avoid poly-DNAs degradation in complex in vivo environment. NK cells were also stained with 1,1′-dioctadecyl-3,3,3′,3′-tetramethylindodicarbocyanine,4-chlorobenzenesulfonate salt (DID), a far-red plasma membrane fluorescent probe, for in vivo location. The as-obtained $IDEAL_{PT}\text{-}NK_{DID}$ cells were intravenously administrated to subcutaneous A549 tumor bearing mice for in vivo application of NK cell

adoptive therapy, DOX and DID fluorescence were imaged in vivo to trace the delivery of IDEAL$_{PT}$-NK$_{DID}$ cells, which were both clearly observed at 3 h after intravenous injection and remained stable until 48 h (Fig. S19). DOX and DID fluorescence were coincided well in vivo, indicating efficient accumulation of IDEAL$_{PT}$-NK$_{DID}$ cells at tumor position. Ex vivo images of mice tumors and other major organs that collected at 24 h after IDEAL$_{PT}$-NK$_{DID}$ cells administration also showed strongest DID and DOX fluorescence in tumor, verified the remarkable tumor-targeting capability of adoptive IDEAL-NK cells (Fig. 4A, IDEAL$_{PT}$-NK$_{DID}$). Control groups were set by intravenously administrating tumor baring mice with PLGA$_{drugs}$ NPs, IL-NK$_{DID}$ cells that in the absence of drugs loading, and NK$_{DID}$-PLGA$_{drugs}$ cells that in the absence of DNA scaffold encapsulation respectively. Due to the tumor-homing driven accumulation, IDEAL$_{PT}$-NK$_{DID}$ cells administrated mice group showed higher DOX fluorescence from tumor position compared to PLGA$_{drugs}$ direct administration group (Fig. 4A, DOX; Fig. S20A, PLGA$_{drugs}$, IDEAL$_{PT}$-NK$_{DID}$). IDEAL$_{PT}$-NK$_{DID}$ cells administrated mice group also showed higher DID fluorescence from tumor position compared with both IL-NK$_{DID}$ cells administration group and NK$_{DID}$-PLGA$_{drugs}$ cells administration group (Fig. 4A, DID; Fig. S20B, IL-NK$_{DID}$, NK$_{DID}$-PLGA$_{drugs}$, IDEAL$_{PT}$-NK$_{DID}$), indicating more efficient accumulation and infiltration of adoptive NK cells in tumor position. These results confirmed the contributions of proceeding chemotherapy to adoptive NK cell infiltration and DNA scaffold encapsulation to adoptive NK cell activity.

To visualize NK cell decapsulation in vivo, IDEAL$_{PT/Cy5/BHQ3}$-NK cells with self-quenched Cy5 fluorescence were prepared with poly-DNA1$_{PT/Cy5}$ and IL-21 APs$_{BHQ3}$. Poly-DNA1$_{PT/Cy5}$ was prepared with P1a$_{PT/Cy5}$ strand that labelled with Cy5, and IL-21 APs$_{BHQ3}$ was prepared with GSH responsive L1$_{PT/BHQ3}$ strand that contains GSH responsive disulfide bond and labelled with BHQ3. P1a$_{PT/Cy5}$ strand and L1$_{PT/BHQ3}$ strand were hybridized in DNA scaffold to quench Cy5 fluorescence (Fig. 4B). GSH efflux cleaved disulfide bond in L1$_{PT/BHQ3}$ to liberate NK cells and recover Cy5 fluorescence, which indicated NK cell liberation and activation. Cy5 fluorescence was obviously shown in vivo at tumor position at 4 h post intravenous administration of IDEAL$_{PT/Cy5/BHQ3}$-NK cells (Fig. S21), indicating the efficient decapsulation of NK cells in tumor microenvironment. Considering the gradual process of GSH efflux and metabolization of detached DNA strands, Cy5 fluorescence intensity remained at slow increase tendency during 12 h. Though IDEAL$_{PT/Cy5/BHQ3}$-NK cells had certain distribution in liver (Fig. 4C, S22, DOX, liver), ex vivo imaging barely demonstrated Cy5 fluorescence recovery from liver (Fig. 4C, S22, Cy5, liver). These results indicated structural integrity of DNA scaffold in systematic circulation and confirmed the

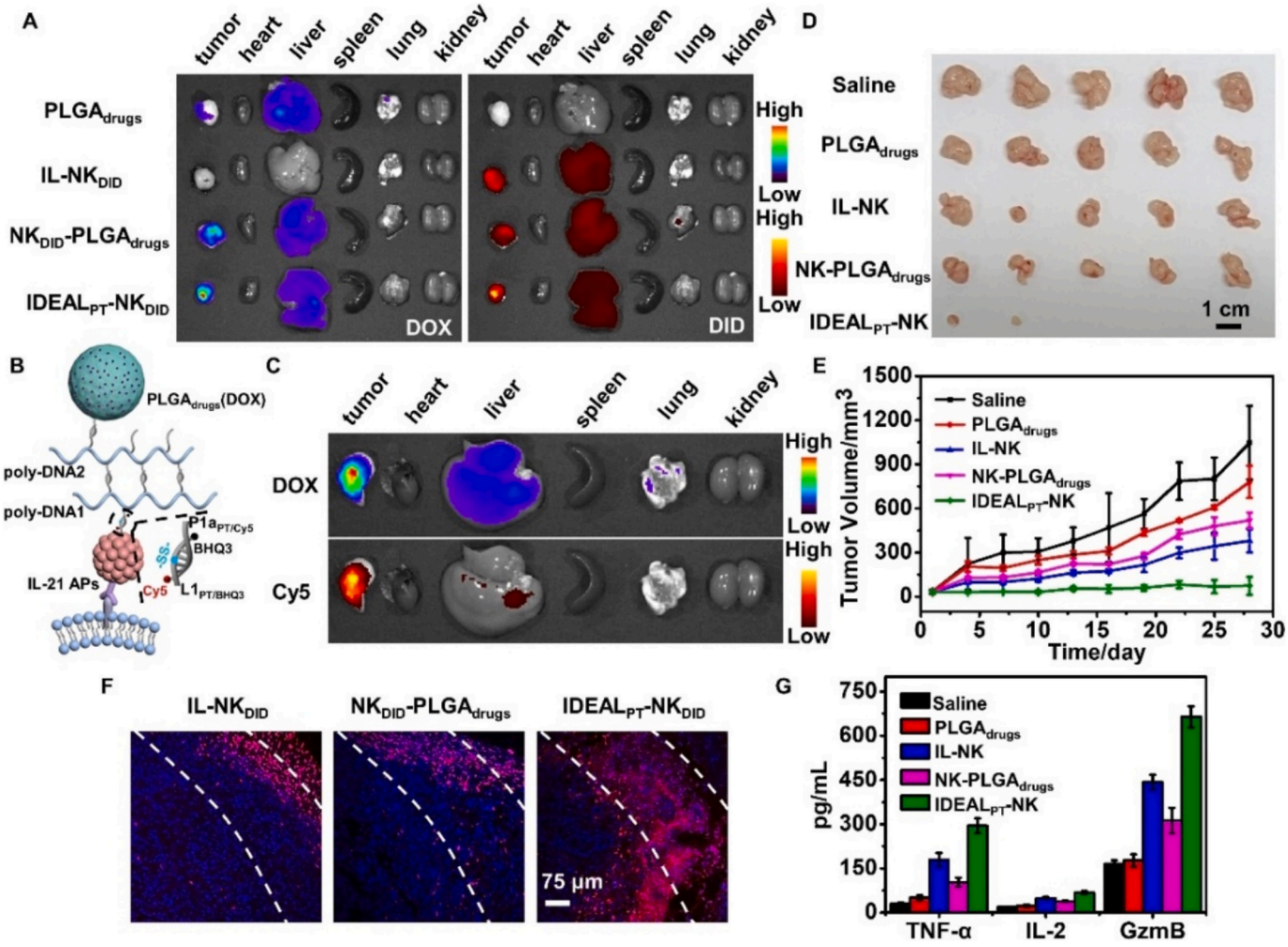

Fig. 4. The antitumor efficacy of IDEAL$_{PT}$-NK cells in vivo. (A) Ex vivo imaging of tumor and organs distributions of PLGA$_{drugs}$ (labelled with DOX) and NK cells (labelled with DID) for PLGA$_{drugs}$ NPs, IL-NK$_{DID}$ cells, NK$_{DID}$-PLGA$_{drugs}$ cells and IDEAL$_{PT}$-NK$_{DID}$ cells administrated mice group respectively. (B) Schematic illustration of IDEAL$_{PT/Cy5/BHQ3}$-NK cells and (C) corresponding DOX and Cy5 fluorescence collected from tumor and organs for IDEAL$_{PT/Cy5/BHQ3}$-NK cells administrated mice. (D) Photographs of dissected A549 mice tumors, and (E) tumor volume change curves for PLGA$_{drugs}$ NPs, IL-NK cells, NK-PLGA$_{drugs}$ cells and IDEAL$_{PT}$-NK cells administrated mice group respectively ($n = 5$). (F) DID fluorescence in tumor sections and (G) secretion of cytotoxic lymphokines (TNF-α, GzmB) and inflammatory cytokines (IL-2) in serum for IL-NK$_{DID}$, NK$_{DID}$-PLGA$_{drugs}$, and IDEAL$_{PT}$-NK$_{DID}$ administrated mice groups.

biosafety of IDEAL-NK cells. $IDEAL_{PT/Cy5/BHQ3}$-NK cells demonstrated strongest intensity for Cy5 fluorescence recovery in tumor position, indicating the efficient accumulation and liberation of NK cells in tumor positions. To visualize $PLGA_{drugs}$ NPs release in vivo, $IDEAL_{PT/TK/BHQ3/Cy5}$-NK cells with self-quenched Cy5 fluorescence were prepared with poly-$DNA2_{PT/TK/BHQ3}$ and $PLGA_{drugs}$ NPs-$N1_{Cy5}$. Poly-$DNA2_{PT/TK/BHQ3}$ was prepared with $P2a_{PT/TK/BHQ3}$ strand that contains ROS responsive TK bond and labelled with BHQ3, and $PLGA_{drugs}$ NPs-$N1_{Cy5}$ was prepared with $N1_{PT/Cy5}$ strand that labelled with Cy5. The control $IDEAL_{PT/nonTK/BHQ3/Cy5}$-NK cells were prepared with poly-$DNA2_{PT/nonTK/BHQ3}$ without TK bond modification. $P2a_{PT/TK/BHQ3}$ strand (or $P2a_{PT/nonTK/BHQ3}$) and $N1_{PT/Cy5}$ strand were hybridized in DNA scaffold to quench Cy5 fluorescence (Fig. S23A). Tumor microenvironment ROS cleaved TK bond in $P2a_{PT/TK/BHQ3}$ to release $PLGA_{drugs}$ NPs and recover Cy5 fluorescence. Compared with $IDEAL_{PT/nonTK/BHQ3/Cy5}$-NK cells group, Cy5 fluorescence in $IDEAL_{PT/TK/BHQ3/Cy5}$-NK cells group was obviously shown in vivo at tumor position (Fig. S23B, C), indicating that tumor microenvironment triggered the efficient release of $PLGA_{drugs}$ NPs in tumor microenvironment. On the contrary, Cy5 fluorescence was barely observed from liver (Fig. S23B, C).

To evaluate the in vivo antitumor effect of $IDEAL_{PT}$-NK cells, the subcutaneous A549 tumor grown mice were randomly divided to 5 groups and intravenously administrated with saline, $PLGA_{drugs}$ NPs, IL-NK cells, NK-$PLGA_{drugs}$ and $IDEAL_{PT}$-NK cells respectively on days 1, 6, and 18. Tumor volume and body weight of mice were monitored every three days until day 28 to evaluate therapeutic effect. $IDEAL_{PT}$-NK cells administrated mice group demonstrated most effective suppression of tumor growth with ~95 % of tumor volume inhibition rate compared with saline administrated mice groups (Fig. 4D, E, Sliane, $IDEAL_{PT}$-NK). IL-NK cells that in the absence of $PLGA_{drugs}$ loading administrated mice group showed ~65 % of tumor volume inhibition rate, indicating the immunotherapy effect solely from NK cells (Fig. 4 D, E, IL-NK). $PLGA_{drugs}$ NPs administrated mice group showed ~26 % of tumor volume inhibition rate, indicating the chemotherapy effect solely from $PLGA_{drugs}$ NPs (Fig. 4D, E, $PLGA_{drugs}$). NK-$PLGA_{drugs}$ cells that in the absence of DNA scaffold encapsulation administrated mice group showed ~52 % of tumor volume inhibition rate (Fig. 4D, E, NK-$PLGA_{drugs}$). Consistent with the above results, we found that intravenous administration of $IDEAL_{PT}$-NK cells apparently prolonged survival (Fig. S24). H&E staining and TUNEL assays at tumor sections also demonstrated most cancer cell apoptosis from $IDEAL_{PT}$-NK cells administrated mice group compared with all the control groups (Fig. S25), confirmed the most effective tumor therapeutic effect. The body weights of all mice groups did not significantly fluctuate during the therapeutic period (Fig. S26). No significant histological toxicity was observed for all the major organs (heart, liver, spleen, lung and kidney) for all the treatment groups (Fig. S27), indicating the biosafety of administrated IDEAL-NK cells.

To further evaluate the contributions of programmed drug release to immunotherapeutic effect of adoptive NK cells, the infiltration of $IDEAL_{PT}$-NK_{DID} cells in solid tumors was evaluated via DID immunohistochemical staining. $IDEAL_{PT}$-NK_{DID} administrated mice group showed strong DID fluorescence intensity from deeper part of the tumor tissue (Fig. 4F, $IDEAL_{PT}$-NK_{DID}). On the contrary, IL-NK_{DID} cells administrated group and NK_{DID}-$PLGA_{drugs}$ cells administrated group only showed DID fluorescence at the edge of tumor tissue with weak fluorescence intensity from tumor interior (Fig. 4F, IL-NK_{DID}, NK_{DID}-$PLGA_{drugs}$). These results confirmed the contributions of chemotherapy and DNA scaffold encapsulation to adoptive immune therapy. The secretion of immune-activation related components, cytotoxic lymphokines (TNF-α, granzyme B) and inflammatory cytokines (IL-2) were also measured in the post-treatment tumor environment via ELISA assays for different mice groups. $IDEAL_{PT}$-NK cells injected mice group demonstrated maximum expressions of TNF-α, granzyme B and IL-2 in sera (Fig. 4G), which explained the better anti-tumor effect achieved by $IDEAL_{PT}$-NK cell therapy.

4. Conclusions

In summary, here we developed a DNA scaffold framed adoptive natural killer cells with programmed drug release for enhanced ACT. NK cells were encapsulated by poly-DNAs framework, and drug-loaded PLGA ($PLGA_{drugs}$) NPs were anchored to DNAs framework to prepare IDEAL-NK cells. During delviery process, poly-DNAs framework effectively blocked the endocytosis of $PLGA_{drugs}$ NPs and correspondingly prevented drug toxicity to NK cells. Tumor microenvironment overexpressed ROS released $PLGA_{drugs}$ NPs for chemotherapy, the corresponding tumor microenvironment remodelling including massive GSH efflux disassembled DNA scaffold and promoted the activity of liberated NK cells. This sequential therapy effectively promoted NK cell infiltration at the tumor site, and showed outstanding inhibitory effects on tumor growth, therefore would have potential clinical applications.

CRediT authorship contribution statement

Shiyi Bi: Writing – original draft, Investigation, Formal analysis, Data curation, Conceptualization. **Jieyu Shen:** Data curation. **Yu Zhu:** Data curation. **Lei Fan:** Supervision. **Huangxian Ju:** Supervision. **Ying Liu:** Writing – review & editing, Supervision, Funding acquisition.

Declaration of competing interest

The authors declare that they have no known competing financial interests or personal relationships that could have appeared to influence the work reported in this paper.

Acknowledgements

We gratefully acknowledge the National Natural Science Foundation of China (22374073), State Key Laboratory of Analytical Chemistry for Life Science (5431ZZXM2204, 5431ZZXM2307).

Appendix A. Supplementary data

Supplementary data to this article can be found online at https://doi.org/10.1016/j.jconrel.2025.113679.

Data availability

Data will be made available on request.

References

[1] C.J. Bashor, I.B. Hilton, H. Bandukwala, D.M. Smith, O. Veiseh, Engineering the next generation of cell-based therapeutics, Nat. Rev. Drug Discov. 21 (9) (2022) 655–675.
[2] T.J. Laskowski, A. Biederstädt, K. Rezvani, Natural killer cells in antitumour adoptive cell immunotherapy, Nat. Rev. Cancer 22 (10) (2022) 557–575.
[3] M.E. Dudley, S.A. Rosenberg, Adoptive-cell-transfer therapy for the treatment of patients with cancer, Nat. Rev. Cancer 3 (9) (2003) 666–675.
[4] M.C. O'Leary, X. Lu, Y. Huang, X. Lin, I. Mahmood, D. Przepiorka, D. Gavin, S. Lee, K. Liu, B. George, W. Bryan, M.R. Theoret, R. Pazdur, FDA approval summary: Tisagenlecleucel for treatment of patients with relapsed or refractory B-cell precursor acute lymphoblastic leukemia, Clin. Cancer Res. 25 (4) (2019) 1142–1146.
[5] N. Bouchkouj, Y.L. Kasamon, R.A. de Claro, B. George, X. Lin, S. Lee, G. M. Blumenthal, W. Bryan, A.E. McKee, R. Pazdur, FDA approval summary: Axicabtagene Ciloleucel for relapsed or refractory large B-cell lymphoma, Clin. Cancer Res. 25 (6) (2019) 1702–1708.
[6] M. Wang, J. Munoz, A. Goy, F.L. Locke, C.A. Jacobson, B.T. Hill, J.M. Timmerman, H. Holmes, S. Jaglowski, I.W. Flinn, P.A. McSweeney, D.B. Miklos, J.M. Pagel, M.-J. Kersten, N. Milpied, H. Fung, M.S. Topp, R. Houot, A. Beitinjaneh, W. Peng, L. Zheng, J.M. Rossi, R.K. Jain, A.V. Rao, P.M. Reagan, KTE-X19 CAR T-cell therapy in relapsed or refractory mantle-cell lymphoma, N. Engl. J. Med. 382 (14) (2020) 1331–1342.
[7] N. Gong, N.C. Sheppard, M.M. Billingsley, C.H. June, M.J. Mitchell, Nanomaterials for T-cell cancer immunotherapy, Nat. Nanotechnol. 16 (1) (2021) 25–36.
[8] M. Zhang, Z. Zhao, Y. Pritykin, M. Hannum, A.C. Scott, F. Kuo, V. Sanghvi, T. A. Chan, V. Seshan, H. Wendel, A. Schietinger, M. Sadelain, M. Huse, Ectopic

activation of the miR-200c-EpCAM axis enhances antitumor T cell responses in models of adoptive cell therapy, Sci. Transl. Med. 13 (2021) eabg4328.
[9] Y. Cheng, Y. Gong, X. Chen, Q. Zhang, X. Zhang, Y. He, L. Pan, B. Ni, F. Yang, Y. Xu, L. Zhou, Y. Yang, W. Chen, Injectable adhesive hemostatic gel with tumor acidity neutralizer and neutrophil extracellular traps lyase for enhancing adoptive NK cell therapy prevents post-resection recurrence of hepatocellular carcinoma, Biomaterials 284 (2022) 121506.
[10] S.S. Yaghoubi, M.C. Jensen, N. Satyamurthy, S. Budhiraja, D. Paik, J. Czernin, S. S. Gambhir, Noninvasive detection of therapeutic cytolytic T cells with 18F–FHBG PET in a patient with glioma, Nat. Clin. Pract. Oncol. 6 (1) (2008) 53–58.
[11] C.H.J. Lamers, S. Sleijfer, S. van Steenbergen, P. van Elzakker, B. van Krimpen, C. Groot, A. Vulto, M. den Bakker, E. Oosterwijk, R. Debets, J.W. Gratama, Treatment of metastatic renal cell carcinoma with CAIX CAR-engineered T cells: clinical evaluation and Management of on-target Toxicity, Mol. Ther. 21 (4) (2013) 904–912.
[12] L. Gandhi, D. Rodríguez-Abreu, S. Gadgeel, E. Esteban, E. Felip, F. De Angelis, M. Domine, P. Clingan, M.J. Hochmair, S.F. Powell, S.Y.S. Cheng, H.G. Bischoff, N. Peled, F. Grossi, R.R. Jennens, M. Reck, R. Hui, E.B. Garon, M. Boyer, B. Rubio-Viqueira, S. Novello, T. Kurata, J.E. Gray, J. Vida, Z. Wei, J. Yang, H. Raftopoulos, M.C. Pietanza, M.C. Garassino, Pembrolizumab plus chemotherapy in metastatic non–small-cell lung Cancer, N. Engl. J. Med. 378 (22) (2018) 2078–2092.
[13] F.S. Hodi, S.J. O'Day, D.F. McDermott, R.W. Weber, J.A. Sosman, J.B. Haanen, R. Gonzalez, C. Robert, D. Schadendorf, J.C. Hassel, W. Akerley, A.J.M. van den Eertwegh, J. Lutzky, P. Lorigan, J.M. Vaubel, G.P. Linette, D. Hogg, C. H. Ottensmeier, C. Lebbé, C. Peschel, I. Quirt, J.I. Clark, J.D. Wolchok, J.S. Weber, J. Tian, M.J. Yellin, G.M. Nichol, A. Hoos, W.J. Urba, Improved survival with Ipilimumab in patients with metastatic melanoma, N. Engl. J. Med. 363 (2010) 711–723.
[14] H.C. Chung, W. Ros, J.-P. Delord, R. Perets, A. Italiano, R. Shapira-Frommer, L. Manzuk, S.A. Piha-Paul, L. Xu, S. Zeigenfuss, S.K. Pruitt, A. Leary, Efficacy and safety of Pembrolizumab in previously treated advanced cervical Cancer: results from the phase II KEYNOTE-158 study, J. Clin. Oncol. 37 (17) (2019) 1470–1478.
[15] R.S. Riley, C.H. June, R. Langer, M.J. Mitchell, Delivery technologies for cancer immunotherapy, Nat. Rev. Drug Discov. 18 (3) (2019) 175–196.
[16] C. Wang, J. Wang, X. Zhang, S. Yu, D. Wen, Q. Hu, Y. Ye, H. Bomba, X. Hu, Z. Liu, G. Dotti, Z. Gu, In situ formed reactive oxygen species–responsive scaffold with gemcitabine and checkpoint inhibitor for combination therapy, Sci. Transl. Med. 10 (2018) eaan3682.
[17] X. Wang, L. Ye, W. He, C. Teng, S. Sun, H. Lu, et al., In situ targeting nanoparticles-hydrogel hybrid system for combined chemo-immunotherapy of glioma, J. Control. Release 345 (2022) 786–797.
[18] A.X. Wang, X.J. Ong, C. D'Souza, P.J. Neeson, J.J. Zhu, Combining chemotherapy with CAR-T cell therapy in treating solid tumors, Front. Immunol. 14 (2023) 1140541.
[19] L. Zitvogel, L. Apetoh, F. Ghiringhelli, G. Kroemer, Immunological aspects of cancer chemotherapy, Nat. Rev. Immunol. 8 (2008) 59.
[20] R.R. Love, H. Leventhal, D.V. Easterling, D.R. Nerenz, Side effects and emotional distress during cancer chemotherapy, Cancer 63 (1989) 604–612.
[21] J.J. Monsuez, J.C. Charniot, N. Vignat, J.Y. Artigou, Cardiac side-effects of cancer chemotherapy, Int. J. Cardiol. 144 (2010) 3e15.
[22] A.-M. Florea, D. Büsselberg, Cisplatin as an anti-tumor drug: cellular mechanisms of activity, drug resistance and induced side effects, Cancers 3 (2011) 1351–1371.
[23] Y. Wang, J. Shi, M. Xin, A.R. Kahkoska, J. Wang, Z. Gu, Cell–drug conjugates, Nat. Biomed. Eng. (2024), https://doi.org/10.1038/s41551-024-01230-6.
[24] J. Xue, Z. Zhao, L. Zhang, L. Xue, S. Shen, Y. Wen, Z. Wei, L. Wang, L. Kong, H. Sun, Q. Ping, R. Mo, C. Zhang, Neutrophil-mediated anticancer drug delivery for suppression of postoperative malignant glioma recurrence, Nat. Nanotechnol. 12 (7) (2017) 692–700.
[25] Z. Luo, Y. Lu, Y. Shi, M. Jiang, X. Shan, X. Li, J. Zhang, B. Qin, X. Liu, X. Guo, J. Huang, Y. Liu, S. Wang, Q. Li, L. Luo, J. You, Neutrophil hitchhiking for drug delivery to the bone marrow, Nat. Nanotechnol. 18 (6) (2023) 647–656.
[26] Y. Chang, X. Cai, R. Syahirah, Y. Yao, Y. Xu, G. Jin, V.J. Bhute, S. Torregrosa-Allen, B.D. Elzey, Y.-Y. Won, Q. Deng, X.L. Lian, X. Wang, O. Eniola-Adefeso, X. Bao, CAR-neutrophil mediated delivery of tumor-microenvironment responsive nanodrugs for glioblastoma chemo-immunotherapy, Nat. Commun. 14 (1) (2023).
[27] M.T. Stephan, J.J. Moon, S.H. Um, A. Bershteyn, D.J. Irvine, Therapeutic cell engineering with surface-conjugated synthetic nanoparticles, Nat. Med. 16 (9) (2010) 1035–1041.
[28] L. Tang, Y. Zheng, M.B. Melo, L. Mabardi, A.P. Castaño, Y.-Q. Xie, N. Li, S. B. Kudchodkar, H.C. Wong, E.K. Jeng, M.V. Maus, D.J. Irvine, Enhancing T cell therapy through TCR-signaling-responsive nanoparticle drug delivery, Nat. Biotechnol. 36 (8) (2018) 707–716.
[29] S. Yang, J. Wen, H. Li, L. Xu, Y. Liu, N. Zhao, Z. Zeng, J. Qi, W. Jiang, W. Han, Y. Zu, Aptamer-engineered natural killer cells for cell-specific adaptive immunotherapy, Small 15 (22) (2019) 1900903.
[30] Y. Luo, Z. Chen, M. Sun, B. Li, F. Pan, A. Ma, J. Liao, T. Yin, X. Tang, G. Huang, Cell-based drug delivery systems participate in the Cancer immunity cycle for improved Cancer immunotherapy, Biomaterials 281 (2022) 121341.
[31] M.D. Mager, V. LaPointe, M.M. Stevens, Exploring and exploiting chemistry at the cell surface, Nat. Chem. 3 (8) (2011) 582–589.
[32] C. Ju, Y. Wen, L. Zhang, Q. Wang, L. Xue, J. Shen, C. Zhang, Neoadjuvant chemotherapy based on Abraxane/human neutrophils Cytopharmaceuticals with radiotherapy for gastric Cancer, Small 15 (5) (2018) 1804191.
[33] [4] Y. Qiu, K. Ren, W. Zhao, Q. Yu, R. Guo, J. He, L. Mei, Y. Liu, J. Tang, S. Xu, J. Li, J. Wei, M. Li, Z. Zhang, Q. He, A "dual-guide" bioinspired drug delivery strategy of a macrophage-based carrier against postoperative triple-negative breast cancer recurrence, J. Control. Release 329 (2021) 191–204.
[34] Y. Huang, Z. Guan, X. Dai, Y. Shen, Q. Wei, L. Ren, J. Jiang, Z. Xiao, Y. Jiang, D. Liu, Z. Huang, X. Xu, Y. Luo, C. Zhao, Engineered macrophages as near- infrared light activated drug vectors for chemo-photodynamic therapy of primary and bone metastatic breast cancer, Nat. Commun. 12 (1) (2021) 4310.
[35] Z. Hussain, M.A. Rahim, N. Jan, H. Shah, M. Rawas-Qalaji, S. Khan, M. Sohail, H. E. Thu, N.A. Ramli, R.M. Sarfraz, M.A.S. Abourehab, Cell membrane cloaked nanomedicines for bio-imaging and immunotherapy of cancer: improved pharmacokinetics, cell internalization and anticancer efficacy, J. Control. Release 335 (2021) 130–157.
[36] G. Deng, Z. Sun, S. Li, X. Peng, W. Li, L. Zhou, Y. Ma, P. Gong, L. Cai, Cell-membrane immunotherapy based on natural killer cell membrane coated nanoparticles for the effective inhibition of primary and abscopal tumor growth, ACS Nano 12 (2018) 12096.
[37] V. Kumar, M. McNerney, A new self: MHC-class-I-independent natural-killer-cell self-tolerance, Nat. Rev. Immunol. 5 (2005) 363–374.
[38] D. Raulet, R. Vance, Self-tolerance of natural killer cells, Nat. Rev. Immunol. 6 (2006) 520–531.
[39] N. Shimasaki, A. Jain, D. Campana, NK cells for cancer immunotherapy, Nat. Rev. Drug Discov. 19 (2020) 200–218.
[40] B. Jason, H. Yoshihiro, S. Mark, N. Stephen, IL-21 induces the functional maturation of murine NK cells, J. Immunol. 172 (2004) 2048–2058.
[41] A.A. van Apeldoorn, H.-J. van Manen, J.M. Bezemer, J.D. de Bruijn, C.A. van Blitterswijk, C. Otto, Raman imaging of Plga microsphere degradation inside macrophages, J. Am. Chem. Soc. 126 (2004) 13226–13227.
[42] M.E.C. Lutsiak, R.T. Semnani, R. De Pascalis, S.V.S. Kashmiri, J. Schlom, H. Sabzevari, Inhibition of CD4+25+ T regulatory cell function implicated in enhanced immune response by low-dose cyclophosphamide, Blood 105 (7) (2005) 2862–2868.
[43] D. Alizadeh, M. Trad, N.T. Hanke, C.B. Larmonier, N. Janikashvili, B. Bonnotte, E. Katsanis, N. Larmonier, Doxorubicin eliminates myeloid-derived suppressor cells and enhances the efficacy of adoptive T-cell transfer in breast Cancer, Cancer Res. 74 (1) (2014) 104–118.
[44] J. Hu, C. Sun, C. Bernatchez, X. Xia, P. Hwu, G. Dotti, S. Li, T-cell homing therapy for reducing regulatory T cells and preserving effector T-cell function in large solid tumors, Clinical Cancer Res. 24 (12) (2018) 2920–2934.
[45] W.J. Lesterhuis, C.J.A. Punt, S.V. Hato, D. Eleveld-Trancikova, B.J.H. Jansen, S. Nierkens, G. Schreibelt, A. de Boer, C.M.L. Van Herpen, J.H. Kaanders, J.H.J. M. van Krieken, G.J. Adema, C.G. Figdor, I.J.M. de Vries, Platinum-based drugs disrupt STAT6-mediated suppression of immune responses against cancer in humans and mice, J. Clin. Invest. 121 (8) (2011) 3100–3108.
[46] C. Qi, J. Gong, J. Li, D. Liu, Y. Qin, S. Ge, M. Zhang, Z. Peng, J. Zhou, Y. Cao, X. Zhang, Z. Lu, M. Lu, J. Yuan, Z. Wang, Y. Wang, X. Peng, H. Gao, Z. Liu, H. Wang, D. Yuan, J. Xiao, H. Ma, W. Wang, Z. Li, L. Shen, Claudin18.2-specific CAR T cells in gastrointestinal cancers: phase 1 trial interim results, Nat. Med. 28 (6) (2022) 1189–1198.
[47] D.W. Loe, R.G. Deeley, S.P. Cole, Verapamil stimulates glutathione transport by the 190-kDa multidrug resistance protein 1 (MRP1), J. Pharmacol. Exp. Ther. 293 (2000) 530–538.
[48] R. Barattin, T. Perrotton, D. Trompier, D. Lorendeau, A.D. Pietro, A.D. M. D'hardemare, H. Baubichon-Cortay, Iodination of verapamil for a stronger induction of death, through GSH efflux, of cancer cells overexpressing MRP1, Bioorg. Med. Chem. 18 (17) (2010) 6265–6274.
[49] J.I. Joo, M. Choi, S.H. Jang, S. Choi, S.M. Park, D. Shin, K.H. Cho, Realizing Cancer precision medicine by integrating systems biology and nanomaterial engineering, Adv. Mater. 32 (35) (2020) 1906783.
[50] M.C. Poznansky, I.T. Olszak, R. Foxall, R.H. Evans, A.D. Luster, D.T. Scadden, Active movement of T cells away from a chemokine, Nat. Med. 6 (2000) 543.
[51] D. Trompier, X.B. Chang, R. Barattin, A. Du Moulinet D'Hardemare, A. Di Pietro, H. Baubichon-Cortay, Verapamil and its derivative trigger apoptosis through glutathione extrusion by multidrug resistance protein MRP1, Cancer Res. 64 (2004) 4950–4956.
[52] K. Block, Y. Gorin, Aiding and abetting roles of NOX oxidases in cellular transformation, Nat. Rev. Cancer 12 (9) (2012) 627–637.
[53] K.M. Cappell, J.N. Kochenderfer, Long-term outcomes following CAR T cell therapy: what we know so far, Nat. Rev. Clin. Oncol. 20 (6) (2023) 359–371.
[54] D. Meng, H. Pan, W. He, X. Jiang, Z. Liang, X. Zhang, X. Xu, Z. Wang, J. Zheng, P. Gong, W. Li, L. Cai, In situ activated NK cell as bio-orthogonal targeted live-cell Nanocarrier augmented solid tumor immunotherapy, Adv. Funct. Mater. 32 (29) (2022) 2202603.